*Progress In Electromagnetics Research, PIER 19, 49–91, 1998*

# THE PROPAGATION AND EXCITATION OF SURFACE WAVES IN AN ABSORBING LAYER

R. T. Ling, J. D. Scholler, and P. Ya. Ufimtsev *

Northrop Grumman Corp.
8900 E. Washington Blvd.
Pico Rivera, CA 90660-3783, USA



## 1. INTRODUCTION

Sommerfeld [1, 2] and his student Zenneck [3] were the earliest investigators of surface waves phenomena as evidenced in their theories of propagation of waves over imperfect conductors. The inhomogeneous plane wave supported by a flat surface separating two infinite homogeneous media has since been known as Zenneck Wave. Initially, the interest was limited to theoretical study until Goubau [4–6] demonstrated

* Also with Electrical Engineering Department, University of California at Los Angeles, Los Angeles, CA 90095-1594

the feasibility of using a transmission wire as a surface waveguide. The phenomena of open-boundary wave-guides that support surface waves have since been studied extensively both experimentally and theoretically. The main characteristic of Zenneck wave is the evanescent (i.e., exponentially decaying) distribution of field structure over the wave front in the transverse plane and the tilting of the equi-phase surfaces due to the losses in the supporting surface which causes a progressive decrease in the amplitude of the wave as it propagates along the interface. This tilting of the wave front provides a component of power to be directed into the surface. It has also been shown [7, 8] that the Zenneck wave is excited by an inhomogeneous plane wave incident on a flat surface at a complex Brewster angle without reflection. The complex incident angle can arise for example from an ordinary, homogeneous plane wave limited by an aperture. The origin of the complex incident angle can be explained by the concept of plane wave spectrum introduced by Booker and Clemmow [9, 10], and Clemmow [11]. These authors have called the inhomogeneous plane wave with complex incident angles (or equivalently with propagation coefficients exceeding that of free space) as an evanescent or a reactive wave [9]. Such waves produce surface waves when incident upon an interface separating two media.

Most theoretical studies on surface waves are concerned with nearly perfect dielectric and non-magnetic media. Goubau [4] and Attwood [12] have analyzed TM-type waves propagating over planar and cylindrical conductors of circular cross section and coated with a thin layer of dielectric material. The surface waves in their studies are characterized by exponentially decaying fields in the direction normal to and away from the guiding structure. In Attwood's treatment the coating material is assumed to be perfectly dielectric and non-magnetic so that the resultant propagation constant of the surface wave and the transverse wave number in the dielectric film are purely real while the transverse wave number in the adjoining free space is purely imaginary. The latter entails the existence of exponentially decaying fields outside the guiding structure. Though Attwood computed dielectric film loss due to Joule heating in terms of $\sigma E^2$ where $\sigma$ is the electrical conductivity and $E$ is the electric field strength, the field quantities were computed with the assumption of purely real dielectric constant. The presence of finite conductivity in the dielectric film which would necessitate a non-vanishing imaginary part in the dielectric constant

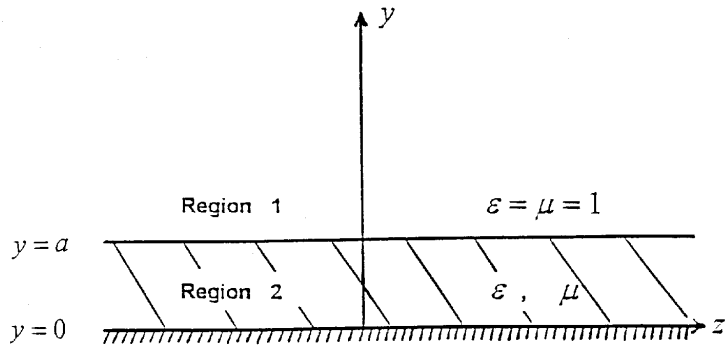


**Figure 1.** Absorbing layer $(0 \leq y \leq a)$ backed up by a perfectly conducting plane $(y = 0)$.

was treated as a small perturbation and ignored in the solution of the field quantities. This approximating perturbation technique is justified when the imaginary part of the dielectric constant is small compared to the real part. In Attwood's treatment, the dielectric material has a loss tangent of 0.001, thus satisfying this condition. In the following, we generalize Attwood's treatment to lossy dielectric and magnetic media without using the perturbation technique. Both the permittivity (or dielectric constant) and permeability are assumed complex. The resultant propagation constant and transverse wave numbers are therefore complex.

For an aperture-limited plane wave incident on an interface, the solution of the diffraction problem can be represented mathematically as a linear combination of plane waves with different incident angles including complex ones. Those plane wave components with complex incident angles can give rise to Zenneck waves type surface waves. Booker and Clemmow [9, 10], and Cullen [13] have given rigorous and mathematically equivalent solutions (as shown in Barlow and Brown [8]) to the launching of Zenneck waves. In the following, we extend their theories to more general cases involving transverse standing waves/longitudinal surface waves in the film excited by aperture-limited plane waves on planes coated with lossy material. Note also that the excitation of surface waves in stratified media is considered in Reference [16].

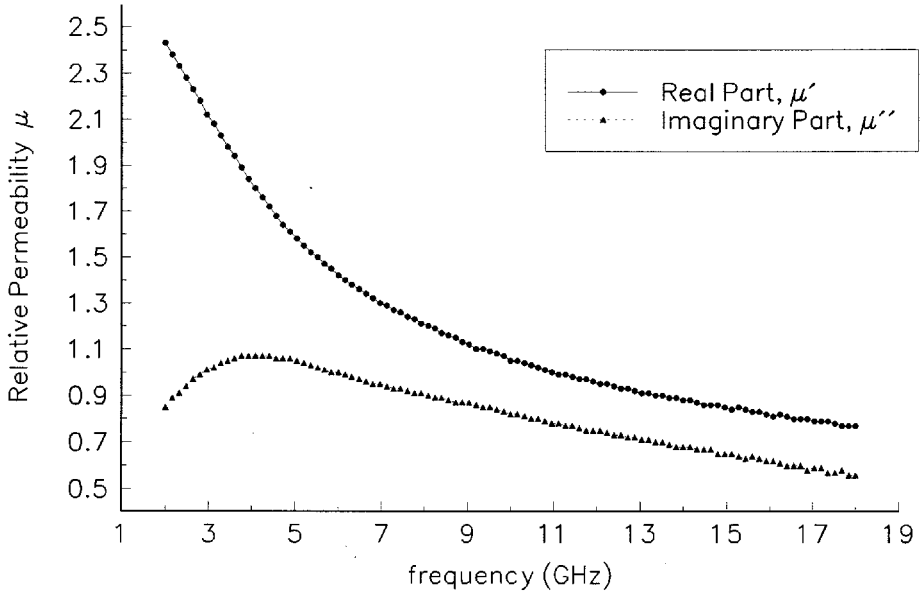


**Figure 2.** Constitutive properties of sample material (Constant relative permittivity: $\epsilon' = 20.45,\ \epsilon'' = 0.73$ ).

## 2. FIELD COMPONENTS AND THE DISPERSION EQUATION FOR SURFACE WAVES

A perfect conductor is assumed to lie on the $x$ - $z$ plane (Fig. 1) over which a thin lossy dielectric and magnetic film of thickness $a$ and relative dielectric constant $\varepsilon = \varepsilon' + i\varepsilon''$ and relative magnetic permeability, $\mu = \mu' + i\mu''$ is coated. Outside of the thin film is the free space or air (Region 1, $\varepsilon = \mu = 1$ ). The absolute permittivity and permeability in the lossy film (Region 2) are denoted by $\varepsilon_2 = \varepsilon_0\varepsilon$ and $\mu_2 = \mu_0\mu$ where $\varepsilon_0$ and $\mu_0$ are the vacuum permittivity and permeability. All the numerical data presented in this paper are obtained for realistic lossy films with complex relative parameters measured in the frequency band 2 to 18 GHz. The complex permittivity in this frequency range is nearly constant, $\varepsilon' = 20.45$ and $\varepsilon'' = 0.73$ . The complex permeability shown in Fig. 2 is frequency dependent. The measured data contained in Fig. 2 are consistent with the Kramers-Kronig relations. A time dependence $\exp(-i\omega t)$ is assumed and suppressed below.

A TM-type surface wave propagating along the $z$-axis is investigated. The field quantities are assumed to be independent of the coordinate $x$. The non-vanishing field components which satisfy the Maxwell equations can be deduced as follows. In the free space (Region 1), $y \geq a$, they are given by

$$H_x = e^{ik_1(y-a)} e^{i\beta z},$$

$$E_y = -\frac{\beta}{k_0} Z_0 H_x, \qquad E_z = \frac{k_1}{k_0} Z_0 H_x, \tag{1}$$

and inside the layer (Region 2), $0 \leq y \leq a$, by

$$H_x = \frac{\cos(k_2 y)}{\cos(k_2 a)} e^{i\beta z},$$

$$E_y = -\frac{\beta}{k_0 \varepsilon} Z_0 H_x, \qquad E_z = i\frac{k_2}{k_0 \varepsilon} Z_0 H_x \tan(k_2 y). \tag{2}$$

In these equations, $k_0 = \omega\sqrt{\varepsilon_0 \mu_0}$ and $Z_0 = \sqrt{\mu_0/\varepsilon_0}$ are the wave number and impedance of the free space. The quantities $k_1$ and $k_2$ are the transverse wave numbers of the wave field outside and inside the layer, respectively. The quantity $\beta$ is the longitudinal wave number, or the propagation constant. These wave numbers are connected by the relations

$$k_1^2 + \beta^2 = k_0^2, \qquad k_2^2 + \beta^2 = k_0^2 \varepsilon \mu \tag{3}$$

through the Helmholtz wave equation. It follows that

$$k_2^2 - k_1^2 = k_0^2(\varepsilon\mu - 1). \tag{4}$$

The $H_x$-components from eqs. (1) and (2) are continuous on the layer surface $(y = a)$. The $E_z$ component satisfies the boundary condition on the perfectly conducting plane $(E_z = 0 \text{ at } y = 0)$ and its continuity at the layer surface, $y = a$, leads to a transcendental relationship

$$k_1 \varepsilon = i k_2 \tan(k_2 a). \tag{5}$$

This transforms into the dispersion equation

$$D(k_0, \beta) \equiv \sqrt{k_0^2 \varepsilon\mu - \beta^2} \tan\left(a\sqrt{k_0^2 \varepsilon\mu - \beta^2}\right) + i\varepsilon\sqrt{k_0^2 - \beta^2} = 0 \tag{6}$$

with the substitutions of $k_1$ and $k_2$ from eq. (3). Note that the ratio of components $E_z$ and $H_x$ on the layer's surface ($y = a$) can be interpreted as the surface impedance

$$Z_s = -\frac{E_z}{H_x} = -Z_0 \frac{k_1}{k_0} \qquad \text{(Ohm)}. \tag{7}$$

For TM-surface waves this impedance must be inductive ($\mathrm{Im}(k_1) > 0$) in order to provide the field concentration above the layer near its surface.

For a given frequency and layer thickness, the dispersion equation (6), and wave numbers equations (3) and (4) can be solved for the unknowns $\beta, k_1$, and $k_2$. Let $\beta = \beta' + i\beta'', k_1 = k_1' + ik_1''$, and $k_2 = k_2' + ik_2''$. The numerical solution involves a two step process. Each step is an iterative procedure to arrive at a final set of solutions from some initial trial values. In the first step, we aim at obtaining an approximate solution by setting the imaginary parts $\varepsilon''$ and $\mu''$ to zero. This is equivalent to assuming that the thin film is non-absorbing. This is the same assumption made in Reference [12]. Under this assumption, $k_2$ becomes purely real, $k_2 = k_2'$, and $k_1$ purely imaginary, $k_1 = ik_1''$. In this case, eqs. (4) and (5) reduce to

$$(k_2')^2 + (k_1'')^2 = k_0^2(\varepsilon'\mu' - 1), \tag{8}$$

$$k_1''\varepsilon' = k_2' \tan(k_2' a) \tag{9}$$

corresponding to eqs. (31) and (33) in Reference [12].

Let $k_2'$ and $k_1''$ be the $x$ and $y$ coordinates on a two dimensional $x$ - $y$ plane. Then eq. (8) represents a circle with a radius given by the square root of the right hand side. Equation (9) represents a tangent-type curve. The intersection point of these two curves is a solution of the coupled equations. If a point representing the trial values of $k_2'$ and the corresponding $k_1''$; computed from eq. (9) is found to lie outside the circle according to eq. (8), a slightly smaller new trial value is set at $0.99k_2'$. If the point is found to lie inside the circle, a slightly larger trial value is set at $1.01k_2'$. The iterative process continues until a sufficiently accurate intersection point is found.

These coordinates of the intersection point along with $k_2'' = 0$ and $k_1' = 0$ are then used as the initial trial values in the second step of the numerical solution using

$$k_1^{n+1} = i\frac{k_2^n}{\varepsilon} \tan(k_2^n a), \tag{10}$$

$$(k_2^{n+1})^2 = (k_1^{n+1})^2 + k_0^2(\varepsilon\mu - 1) \tag{11}$$

to advance the solution from $n^{th}$ to $(n+1)^{th}$ iteration repetively until the solution sufficiently converges. Numerical calculations are carried out for frequencies ranging from 2 to 18 GHz, and layer thickness ranging from 0.05 to 0.09 inch. The transverse distribution of the field inside the layer is determined by the wave number $k_2$. It is shown by numerical computations that all values of $k_2'a$ are less than $\pi/2$. This implies that for these frequencies and layer thicknesses, only the single (fundamental) mode solution exists.

## 3. ATTENUATION AND LOSSES OF SURFACE WAVES INSIDE ABSORBING LAYERS

The imaginary part of the propagation constant $\beta = \beta' + i\beta''$ determines the attenuation factor $|\exp(i\beta z)| = \exp(-\beta'' z)$ in eqs. (1) and (2) for the surfaces waves. The complex quantity, $\beta$ is obtained numerically from the dispersion relations as described in the previous Section. In principle, the attenuation constant $\beta''$ should be equal to the sum of two components $\alpha_e$ and $\alpha_m$ which account for the electric and magnetic losses, respectively. They are defined by

$$\alpha_e = \frac{P_e}{2P_z}, \qquad \alpha_m = \frac{P_m}{2P_z}, \qquad (1/\text{meter}) \tag{12}$$

where

$$P_e = \frac{1}{2}\omega\varepsilon_0\varepsilon'' \int_0^a (|E_y|^2 + |E_z|^2)dy, \qquad (\text{Watt/meter}^2) \tag{13}$$

$$P_m = \frac{1}{2}\omega\mu_0\mu'' \int_0^a |H_x|^2 dy, \qquad (\text{Watt/meter}^2) \tag{14}$$

are the total power of electric and magnetic losses inside the layer per unit length in the $z$- direction, and

$$P_z = \frac{1}{2}\text{Re}\left(\int_0^\infty E_y H_x^* dy\right) \qquad (\text{Watt/meter}) \tag{15}$$

is the total power transferred by the surface wave. All these quantities relate to the cross section of the guiding structure with the unit width $(0 \le x \le 1)$, and they are averaged in time for the period of the field

oscillations $(0 \le t \le 2\pi/\omega)$. The substitution of the field components (1), (2) into eqs. (13–15) ieads to the following explicit expressions

$$P_e = \frac{1}{2k_0} Z_0 \frac{\varepsilon''}{|\varepsilon|^2} \frac{1}{|\cos(k_2 a)|^2} \cdot \left[ |\beta|^2 \int_0^a |\cos(k_2 y)|^2 dy + |k_2|^2 \int_o^a |\sin(k_2 y)|^2 dy \right], \quad (16)$$

$$P_m = \frac{1}{2} Z_0 k_0 \mu'' \frac{1}{|\cos(k_2 a)|^2} \cdot \int_0^a |\cos(k_2 y)|^2 dy, \quad (17)$$

$$P_z = \frac{1}{2k_0} Z_0 \frac{1}{|\cos(k_2 a)|^2} \cdot \left[ \frac{\beta'}{2k_1''} |\cos(k_2 a)|^2 dy + \mathrm{Re}\left(\frac{\beta}{\varepsilon}\right) \int_0^a |\cos(k_2 y)|^2 dy) \right] \quad (18)$$

where

$$\int_0^a |\sin(k_2 y)|^2 dy = \frac{1}{4} \left[ \frac{\sinh(2k_2'' a)}{k_2''} - \frac{\sin(2k_2' a)}{k_2'} \right], \quad (19)$$

$$\int_0^a |\cos(k_2 y)|^2 dy = \frac{1}{4} \left[ \frac{\sinh(2k_2'' a)}{k_2''} + \frac{\sin(2k_2' a)}{k_2'} \right]. \quad (20)$$

It is shown numerically that the attenuation constant $\beta''$ solved from the dispersion equation satisfies the exact relation $\beta'' = \alpha_e + \alpha_m$ where the right-hand side is computed from eqs. (12) to (20).

The quantities $\beta'', \alpha_e,$ and $\alpha_m$ are shown in Figures 3, 4, and 5. The magnetic losses apparently dominate. This is in agreement with the well known fact that thin layers with electric losses are not efficient radar absorbing materials when they are placed on metallic plates. This is because of the boundary condition which requires the tangential component of the electric field to vanish on the layer-metal surface.

From Figures 4 and 5, it is seen that electric and magnetic losses ($\alpha_e$ and $\alpha_m$) become maximal at the same frequencies. Figure 6 plots the attenuation constant $\beta''$ as a function of the ratio of layer thickness to wavelength in the medium of the layer, $\lambda_d = \lambda_0/\mathrm{Re}(\sqrt{\varepsilon\mu})$ where $\lambda_0 = 2\pi/k_0$ is the wavelength in the free space. This figure demonstrates the resonance behavior of surfaces waves in the absorbing layer. The maximum absorption occurs when the ratio $a/\lambda_d$ is in the neighborhood of $0.19 - 0.20$.

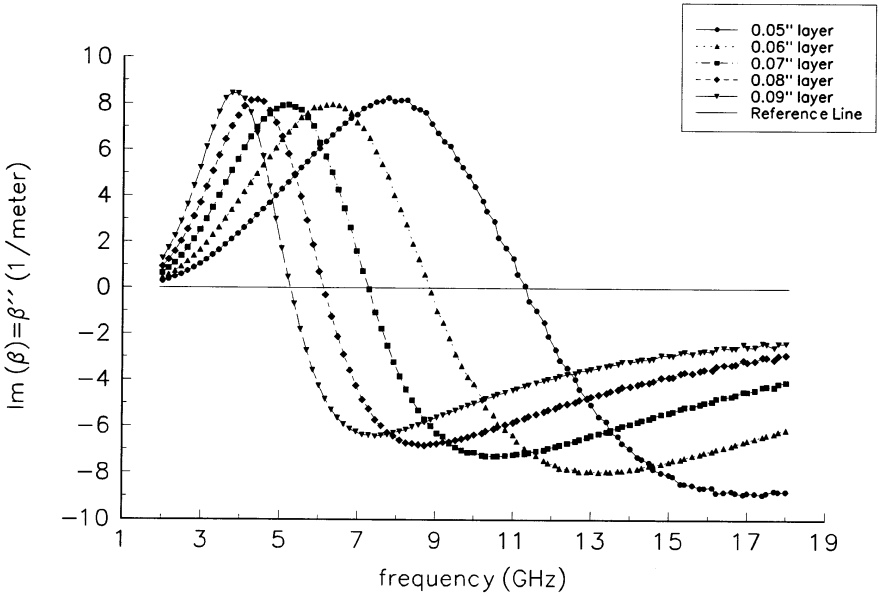


**Figure 3.** Surface wave attenuation constant in absorbing layers.

One might expect that the maximum absorption of the field inside the layer would be accompanied by the maximum concentration of the external field $(y > a)$ near the layer surface $(y = a)$. However, the comparison of Figures 3 and 7 shows that the quantity $k_1''$ which determines the distribution of the field above the layer, reaches maximum values at lower frequencies than the attenuation constant $\beta''$ does. The quantity $k_1'$ is plotted on Fig. 8. Its negative values indicate that the wave above the layer moves towards the layer boundary. Figure 9 shows the quantity $\beta'$ as a function of frequency.

From Figs. 3, 4, and 5, the attenuation constants $\beta''$, $\alpha_e$, and $\alpha_m$ reach their maxima and then decrease with further increase in frequency. They reach the zero values and then becomes negative. Negative values of $\beta'', \alpha_e$, and $\alpha_m$ result from non-physical solutions of the dispersion equation. They imply the amplification of the field, rather than energy absorption, and must be ignored. Physically these negative values mean that surface waves cannot be excited and thus no propagation occurs along the layers. This is also confirmed in Fig. 7 where the quantity $k_1''$ reaches the zero values at the same frequencies as the quantities $\beta'', \alpha_e$, and $\alpha_m$. As the frequency increases, the

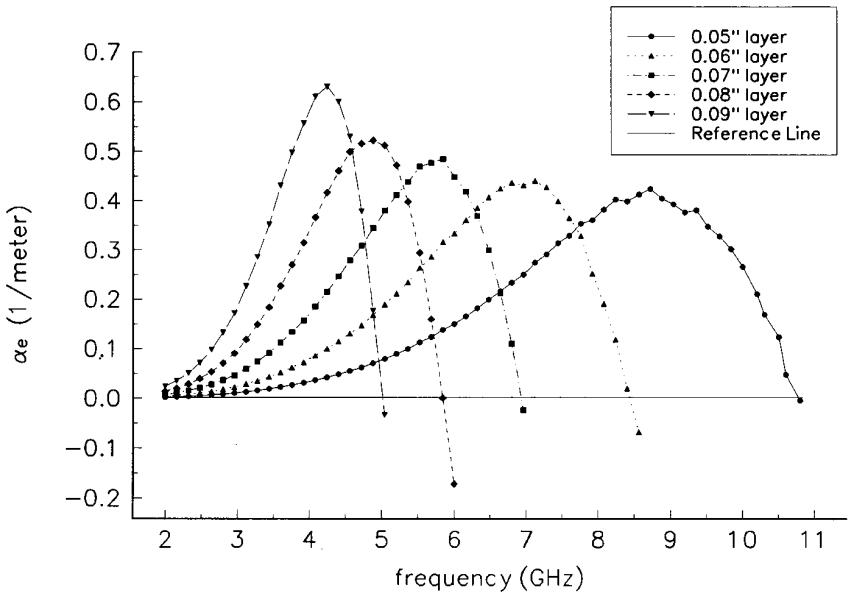


**Figure 4.** Surface wave attenuation factor (Electric loss) in absorbing layers.

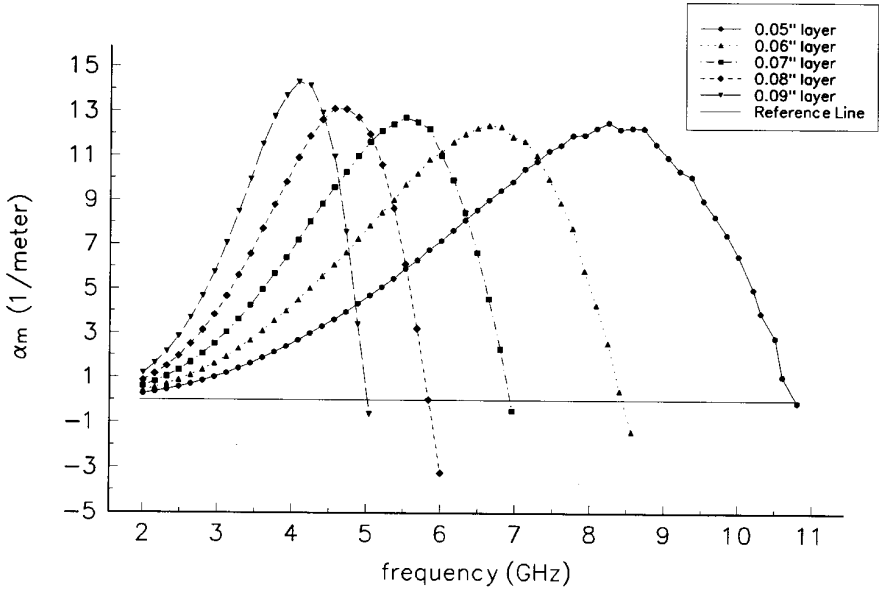


**Figure 5.** Surface wave attenuation factor (Magnetic loss) in absorbing layers.

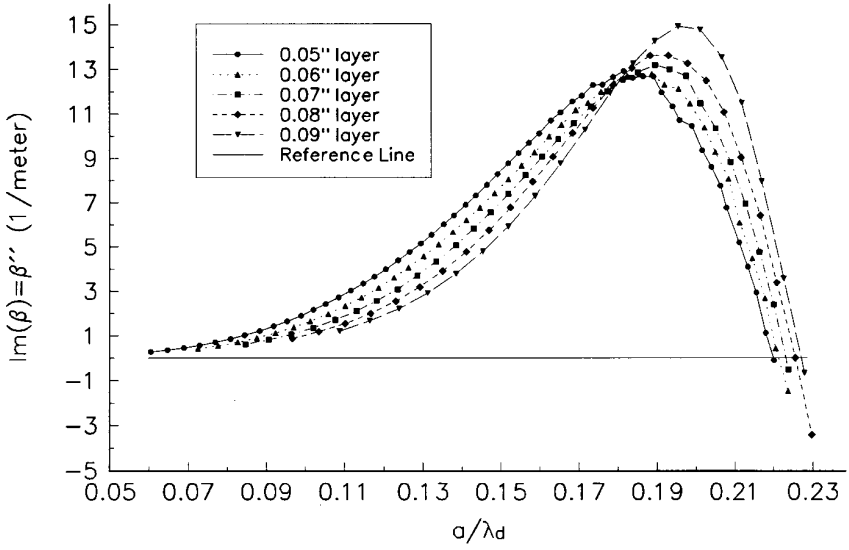


**Figure 6.** Attenuation constant as a function $a/\lambda_d$ in absorbing layers.

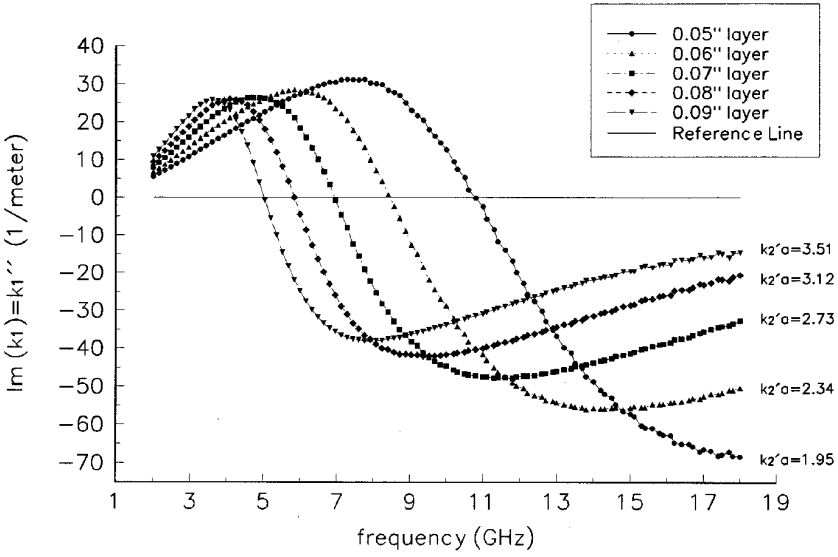


**Figure 7.** Transverse wave numbers in free space (Imaginary part).

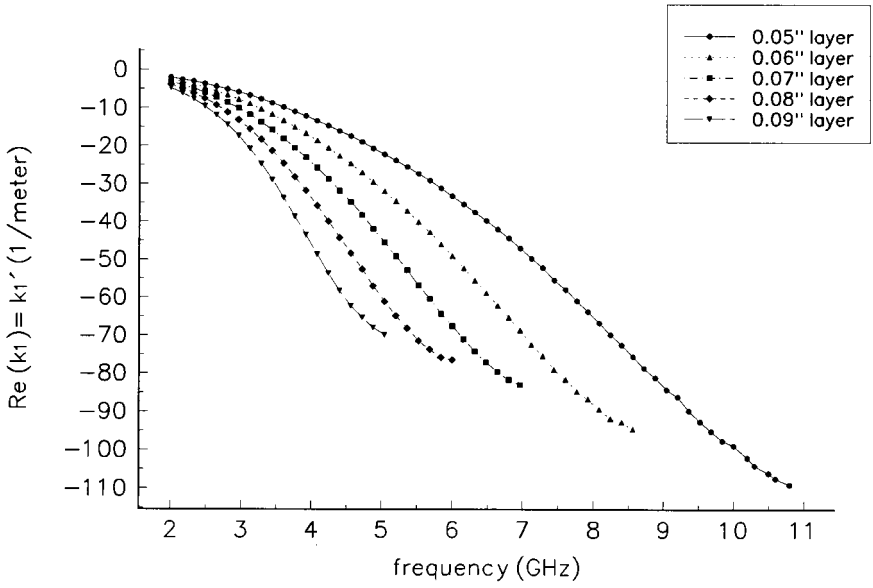


**Figure 8.** Transverse wave numbers in free space (Real part).

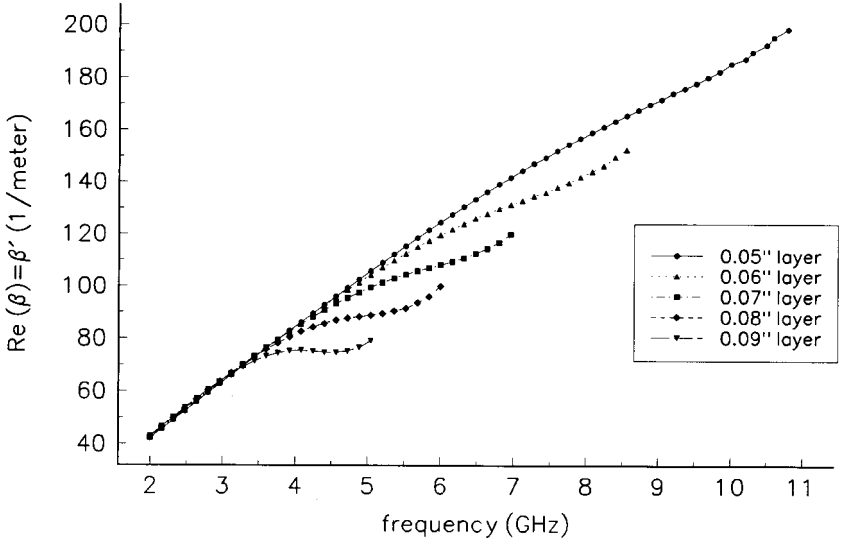


**Figure 9.** Surface wave propagation constant in absorbing layers.

quantity $k_1''$, becomes negative. As a result, in accordance with eq. (7), the surface impedance $Z_s$ becomes capacitive and does not allow the excitation and propagation of TM-surface waves.

The frequency at which the quantities $\beta'', \alpha_e,$ and $\alpha_m$ vanish can be considered as the *upper cutoff frequency.* This is a special feature of surface waves in absorbing layers. In lossless layers surface waves can exist at any high frequency. It is interesting to observe from previous figures that as the layers thicken the upper cutoff frequency decreases and the frequency band widths of the surface wave become narrower. The numerical results presented in this paper, with the exception of Figs. 3 and 7, contain only the values for physical quantities up to just beyond the upper cutoff frequency for each layer. Values further beyond are not physically meaningful.

## 4. PHASE AND AMPLITUTDE FRONTS OF SURFACE WAVES

Equation (1) describes a spatial distribution of the surface wave outside the layer $(y > a)$ with a factor

$$e^{i\phi_p - \phi_a} \quad \text{where} \quad \phi_p = \beta' z + k_1' y, \quad \phi_a = \beta'' z + k_1'' y. \tag{21}$$

For physically allowed solutions below the upper cutoff frequency, the dispersion equations provide the following values: $\beta' > 0$, $\beta'' \geq 0$, and $k_1' \leq 0$, $k_1'' > 0$. Therefore, the surface wave outside the absorbing layer is an inhomogeneous plane wave incident on the layer without reflection. Due to the losses inside the layer this wave undergoes the exponential attenuation in the $z$-direction and its amplitude decreases exponentially along the normal to the layer (in the $y$-direction).

Setting $\phi_p = const$ and $\phi_a = const$ determine the phase and amplitude fronts, respectively:

$$y_p = z_p \tan\gamma_p + const, \quad y_a = z_a \tan\gamma_a + const, \tag{22}$$

where

$$\tan\gamma_p = -\frac{\beta'}{k_1'}, \qquad \tan\gamma_a = -\frac{\beta''}{k_1''}. \tag{23}$$

According to eq. (3) the quantity $k_1^2 + \beta^2$ is purely real. It follows that $\beta'\beta'' + k'k'' = 0$ and

$$\tan\gamma_a = -\frac{\beta''}{k_1''} = \frac{k_1'}{\beta'} = -\cot\gamma_p. \tag{24}$$

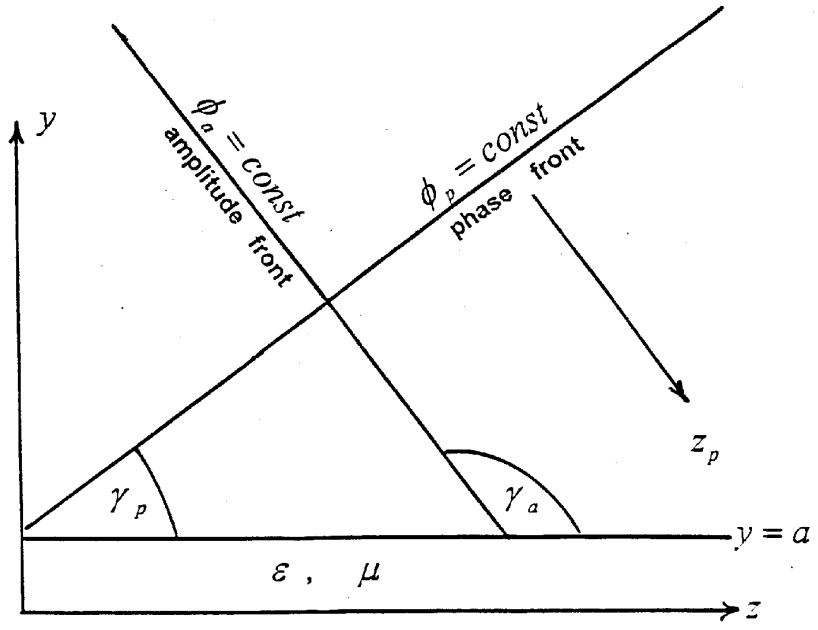


**Figure 10.** Amplitude and phase fronts of the surface wave above the layer.

Therefore, $\gamma_a = \frac{\pi}{2} + \gamma_p$, i.e. outside the layer the phase and amplitude fronts of the surface wave are perpendicular to each other (Fig. 10). This is in agreement with the well known property of inhomogeneous plane waves propagating in lossless media. The angles $\gamma_p$ and $\gamma_a$ are shown in Figs. 11 and 12 as functions of frequency. They acquire minimum values near the upper cutoff frequency.

It is interesting to note a close connection between the angle $\gamma_p$ and the complex Brewster angle $\gamma_B = \gamma'_B + i\gamma''_B$. The latter is introduced by the relation

$$e^{i(\beta z + k_1 y)} = e^{ik_0(z \sin\gamma_B - y\cos\gamma_B)} \tag{25}$$

where

$$\sin\gamma_B = \beta/k_0, \qquad \cos\gamma_B = -k_1/k_0 \tag{26}$$

From these equations it follows that

$$\sin\gamma'_B \cosh\gamma''_B = \beta'/k_0, \qquad \cos\gamma'_b \sinh\gamma''_B = \beta''/k_0,$$

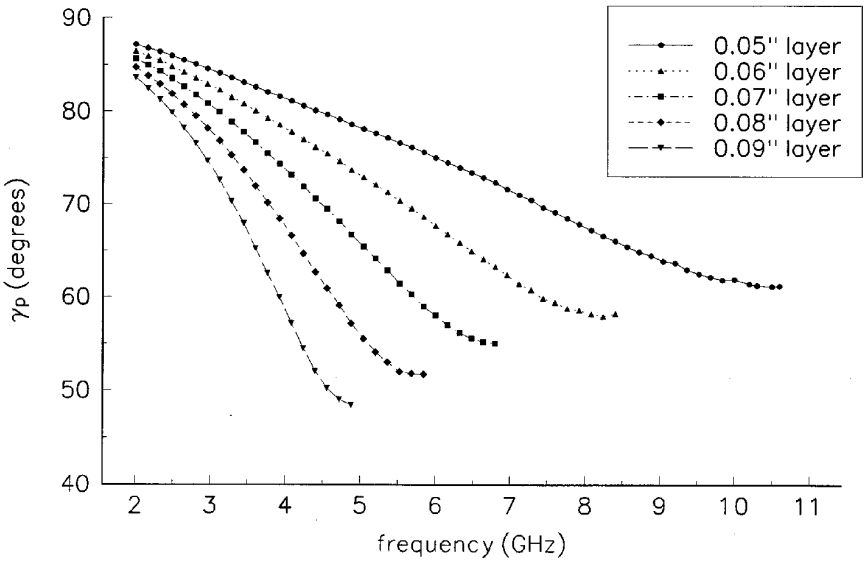


**Figure 11.** Phase front angles outside the layers.

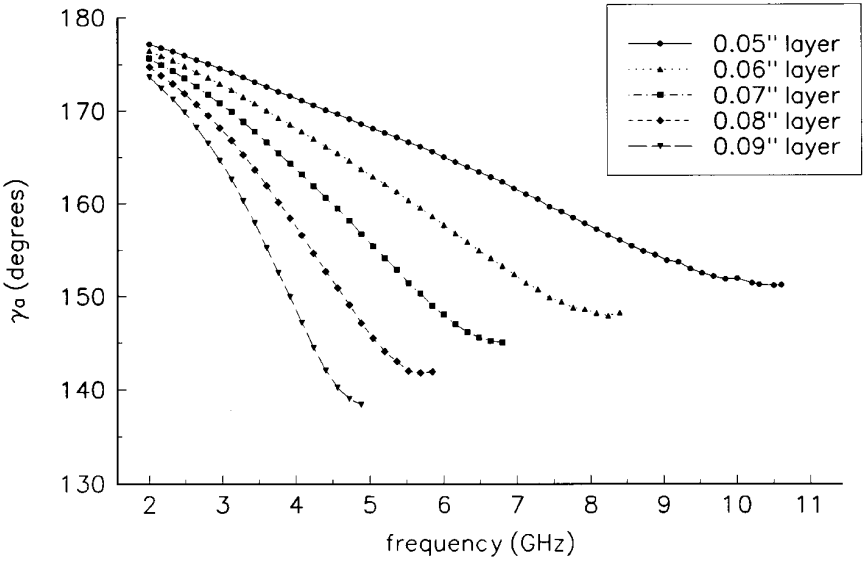


**Figure 12.** Amplitude front angles outside the layers.

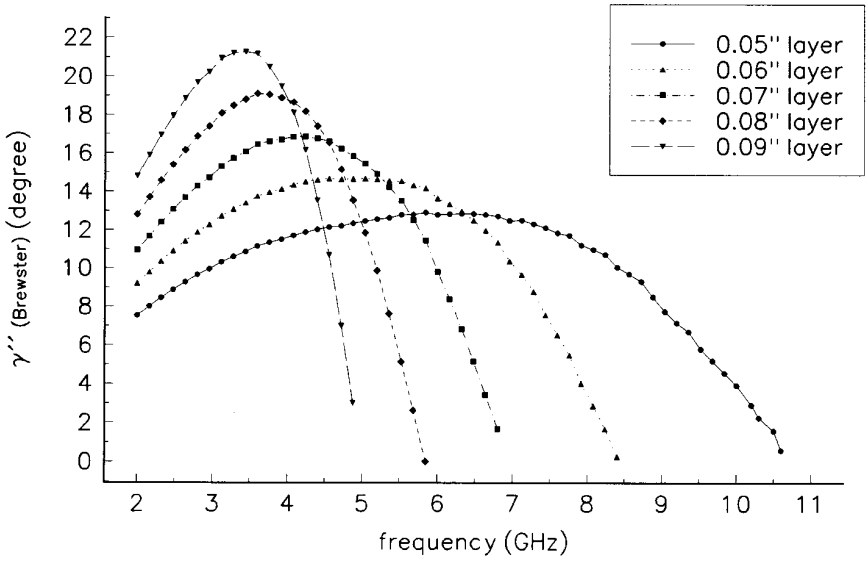


**Figure 13.** Brewster angle (Imaginary part).

$$\cos\gamma'_B \cosh\gamma''_B = -k'_1/k_0, \qquad \sin\gamma'_b \sinh\gamma''_B = k''_1/k_0,$$

and

$$\tan\gamma'_B = -\beta'/k'_1 = k''_1/\beta'', \tag{27}$$

$$\tanh\gamma''_B = -\beta''/k'_1 = k''_1/\beta'. \tag{28}$$

The above mentioned relationship $k'_1 k''_1 + \beta'\beta'' = 0$ leads to the equalities on the right- hand sides of eqs. (27) and (28). Comparison of eqs. (23) and (27) shows that $\gamma'_B = \gamma_p$. Thus, the real part of the Brewster angle exactly equals the angle $\gamma_p$ (Fig. 11). The imaginary part of the Brewster angle found from eq. (28) is plotted on Fig. 13.

Inside the layer, the surface wave is composed of two inhomogeneous plane waves. When the function $\cos(k_2 y)$ in eq. (2) is decomposed into $\exp(\pm i k_2 y)$, we obtain $H_x = H_x^+ + H_x^-$ where

$$H_x^+ = const \cdot e^{i\phi_p^+ - \phi_a^+}, \quad H_x^- = const \cdot e^{i\phi_p^- - \phi_a^-}, \tag{29}$$

with

$$\phi_p^+ = \beta' z + k'_2 y, \qquad \phi_a^+ = \beta'' z + k''_2 y,$$

$$\phi_p^- = \beta' z - k_2' y, \qquad \phi_a^- = \beta'' z - k_2'' y, \tag{30}$$

where $k_2' > 0, k_2'' \geq 0$ from the solution of the dispersion equation. The $H_x^-$-component represents an inhomogeneous plane wave moving forward positively in the $z$-direction and negatively in the $y$-direction. The $H_x^+$ component moves positively in both $y$- and $z$- directions. Consequently the surface wave in the layer is a criss-cross pattern. Such waves are often referred to as the Brillouin waves.

Equations for the phase and amplitude fronts $\phi_p^\pm = const, \phi_a^\pm = const$ can be written in the standard form $y = z \tan\gamma + const$ with

$$\tan\gamma_p^- = -\tan\gamma_p^+ = \frac{\beta'}{k_2'}, \quad \tan\gamma_a^- = -\tan\gamma_a^+ = \frac{\beta''}{k_2''} \tag{31}$$

where $\gamma_p^+ = \pi - \gamma_p^-, \quad \gamma_a^+ = \pi - \gamma_a^-$.

The numerical values for the angles $\gamma_p^-, \gamma_a^-$ are shown in Figs. 14 and 15. Inside the absorbing layer, the phase and amplitude fronts of inhomogeneous plane waves *are not perpendicular* to each other. The angle between them ( $\gamma^- = \gamma_p^- - \gamma_a^-$) is shown in Fig. 16 and does not exceed $11^\circ$ . The lowest value of this angle, about 2.6 degrees, occurs in the layer with 0.09 inch thickness. With respect to the $z$-axis, the slope of the phase and amplitude fronts of inhomogeneous plane waves does not exceed $10.5^\circ$ . A special feature of the fields inside the layers consists of a non-monotonic behavior of the angles $\gamma_p^-, \gamma_a^-$, and $\gamma_p^- - \gamma_a^-$ as functions of frequency. The thicker the layers, the faster these angles change.

## 5. PHASE AND ENERGY VELOCITIES OF SURFACE WAVES

According to eq. (21) the phase front of the surface wave outside the layer moves along the amplitude front in the direction

$$\overrightarrow{z}_p = \hat{z}\sin\gamma_p - \hat{y}\cos\gamma_p, \tag{32}$$

as shown in Fig. 10. The phase factor of the surface wave is determined by $\exp(i\phi_p)$ where

$$\phi_p = z_p(\beta' \sin\gamma_p - k_1' \cos\gamma_p) = z_p\sqrt{\beta'^2 + k_1'^2}. \tag{33}$$

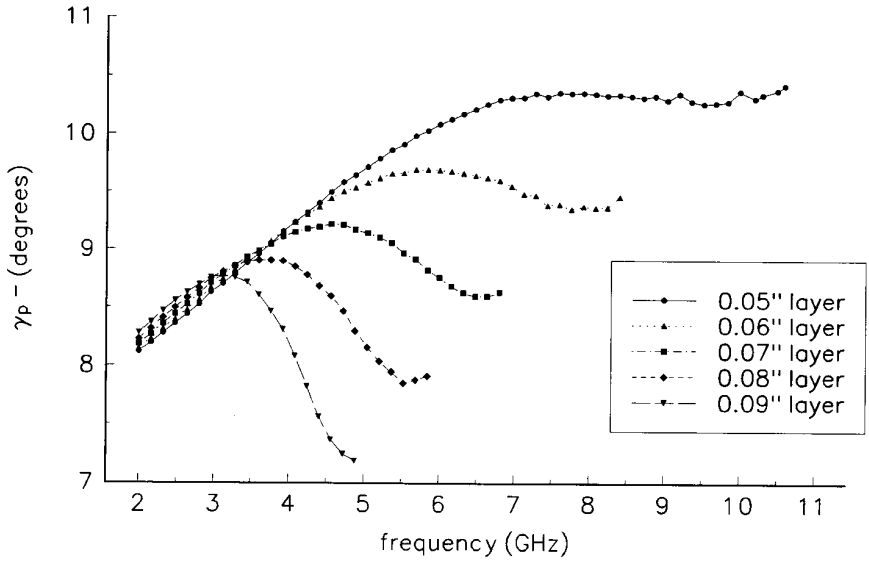


**Figure 14.** Phase front angles inside the layers.

Therefore, the phase velocity equals

$$\overrightarrow{\mathcal{V}}_p = \hat{z}_p \frac{\omega}{\sqrt{\beta'^2 + k_1'^2}}. \tag{34}$$

One should emphasize that the phase velocity is oriented in the $\hat{z}_p$-direction (*not in the* $z$*-direction along the layer*). Figure 17 shows that the quantity is less than the light velocity $(c = 1/\sqrt{\varepsilon_0 \mu_0})$ in free space. The $z$-component of the phase velocity

$$(\overrightarrow{\mathcal{V}}_p \cdot \hat{z}) = \mathcal{V}_p \sin\gamma_p = \frac{\omega\beta'}{k_1'^2 + \beta'^2} \tag{35}$$

is plotted on Fig. 18. In contrast to the total phase velocity defined by eq. (34), its $z$-component as given by eq. (35) is nearly a monotonic decreasing function which reaches minimum values near the upper cutoff frequency due to the multlpiler $\sin\gamma_p$ with the angle $\gamma_p$ being shown in Fig. 11.

Equations (34) and (35) are completely different from the conventional definition of the phase velocity along the guiding structure,

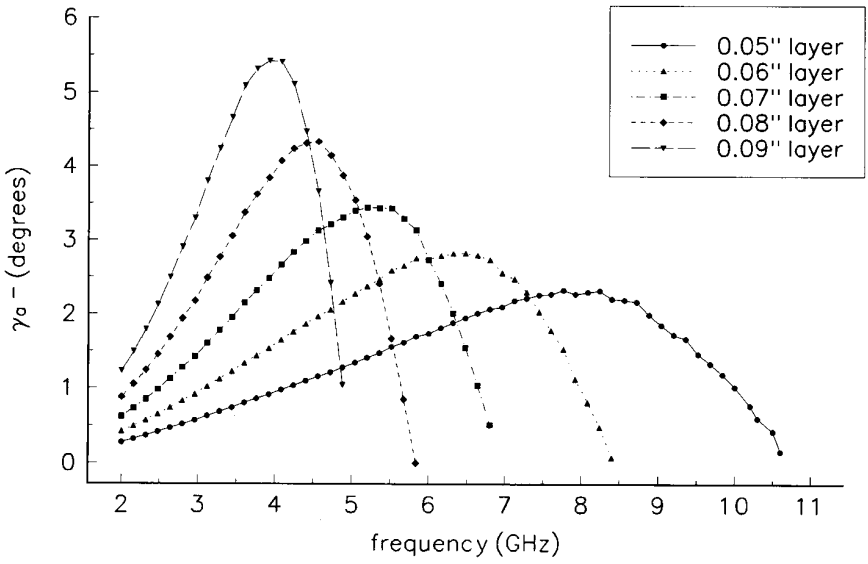


**Figure 15.** Amplitude front angles inside the layers.

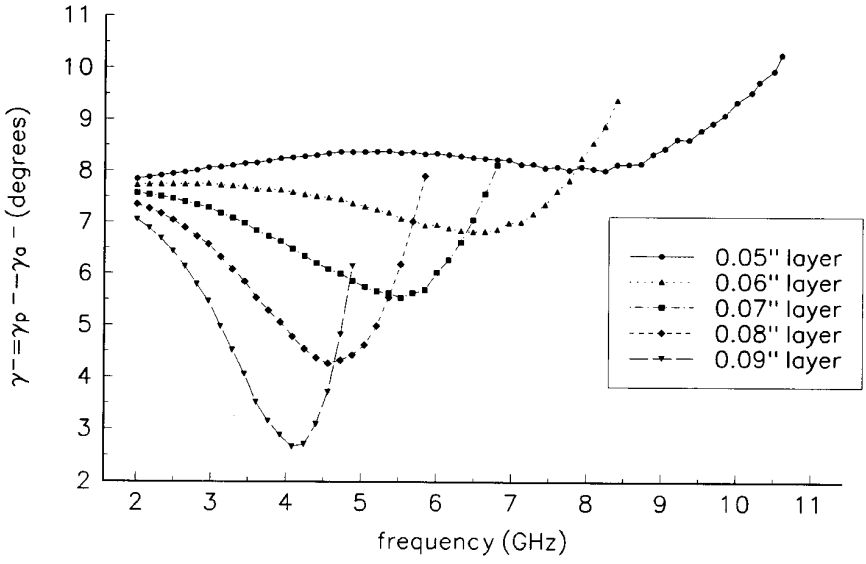


**Figure 16.** Angles between phase front and amplitude front inside the layers.

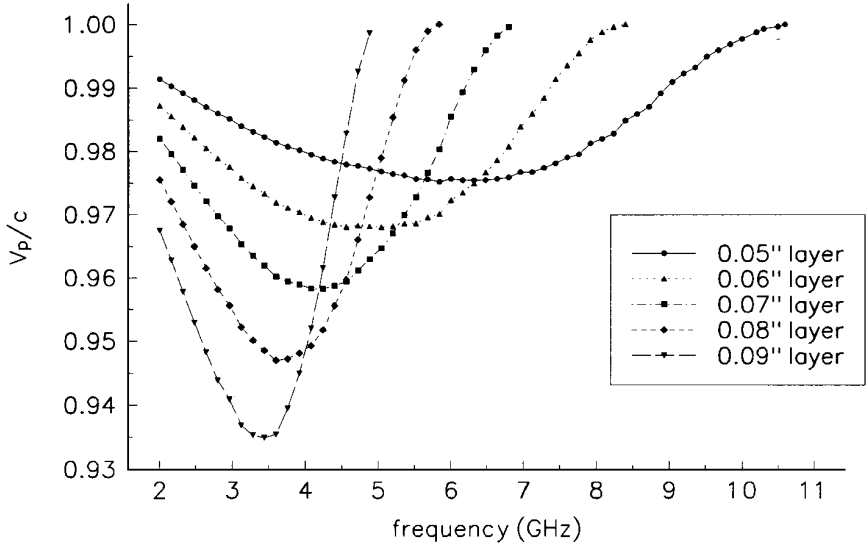


**Figure 17.** Phase velocity of surface waves outside the layers.

$\overrightarrow{\mathcal{V}}_p^{con} = (\omega/\beta')\hat{z}$ . The latter is not applicable in the case of lossy layers considered here and gives values which can exceed the light velocity $c$ (Fig. 19). At the upper cutoff frequency when $\beta = \beta'$ , $k_1 = k_1'$ , and $k_1'^2 + \beta'^2 = k_0^2$ , eq. (35) reduces to $(\overrightarrow{\mathcal{V}}_p \cdot \hat{z}) = c^2/\mathcal{V}_p^{con}$ .

Inside the layer the surface wave consists of two inhomogeneous plane waves (Eq. (29)). Their phase velocity in the direction of the phase front propagation *(not in the direction along the layer)* is determined by the expression

$$\mathcal{V}_p^+ = \mathcal{V}_p^- = \frac{\omega}{\sqrt{\beta'^2 + k_2'^2}}. \tag{36}$$

similar to (34). Numerical values show that this quantity does not depend on the layer thickness (Fig. 20) below the corresponding cutoff frequency. One can see also that it differs from the ratio $\mathcal{V}_d/c = 1/\mathrm{Re}(\sqrt{\varepsilon\mu})$ shown in the same figure by less than 10%. The quantity $\mathcal{V}_d$ can be interpreted as the light velocity in a medium with the refractive index $n = \mathrm{Re}(\sqrt{\varepsilon\mu})$ .

One notes an interesting behavior of surface waves near the upper cutoff frequency. As shown in Section 3 and mentioned above,

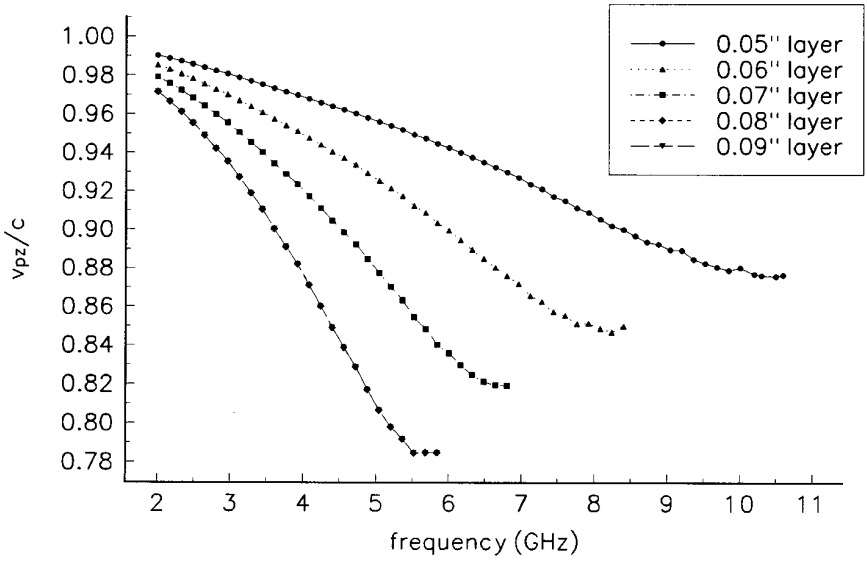


**Figure 18.** The $z$-component of the phase velocity according to eq. (30).

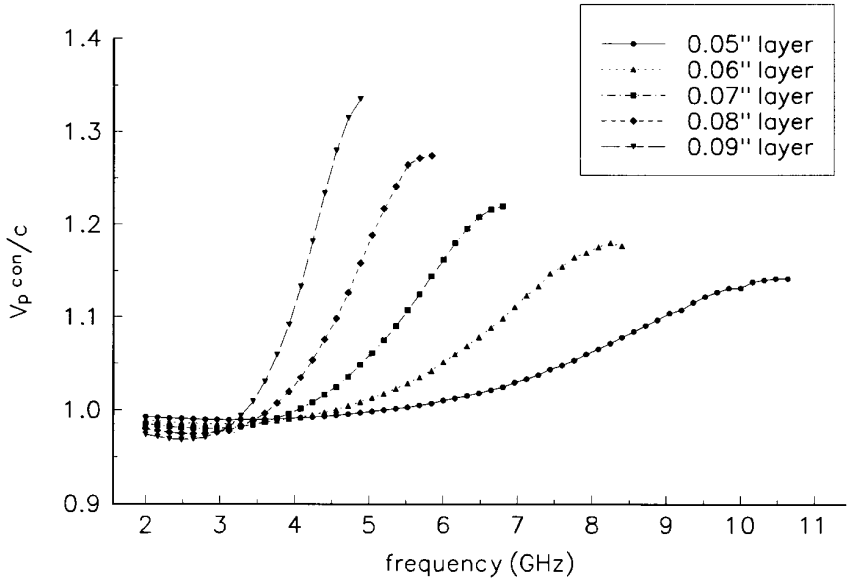


**Figure 19.** Conventional phase velocity.

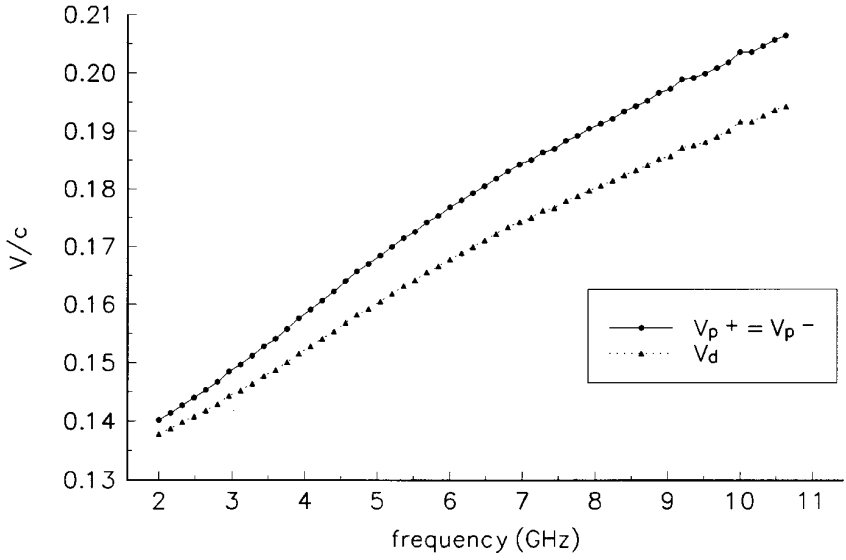


**Figure 20.** Phase velocity and light velocity inside the layers.

at the upper cutoff frequency the propagation constant $\beta$ and transverse wave number $k_1$ become purely real $(\beta = \beta', k_1 = k_1')$, and $\sqrt{\beta'^2 + k_1'^2} = k_0$. Therefore, the phase velocity (34) of the surface wave outside the layer in the $\hat{z}_p$-direction (32) *(not in the z-direction along the layer)* becomes equal to the light velocity, $\mathcal{V}_p = \omega/k_0 = c$ This can be seen in Fig. 17. What actually happens at the upper cutoff frequency is that the surface wave outside the layer transforms into an ordinary plane wave incident on the layer at an oblique angle. For this reason its phase front moves along the layer faster than light.

The time-averaged power density flux vector is given by the Poynting vector

$$\overrightarrow{P} = \frac{1}{2}\mathrm{Re}[\overrightarrow{E} \times \overrightarrow{H}^*]. \tag{37}$$

Outside the layer (Region 1) the surface wave is described by eq. (1). Therefore its Poynting vector contains the components

$$P_y = \frac{k_1'}{2\omega\varepsilon_0} e^{-2[k_1''(y-a)+\beta'' z]}, \qquad P_z = \frac{\beta'}{2\omega\varepsilon_0} e^{-2[k_1''(y-a)+\beta'' z]}. \tag{38}$$

Their ratio is equal to

$$\frac{Pz}{(-P_y)} = -\frac{\beta'}{k_1'} = \tan\gamma_p. \tag{39}$$

This implies that the Poynting vector is directed along the amplitude front in the $z_p$-direction which is normal to the phase front (Fig. 10). In other words, the power flux vector of the surface wave outside the layer is parallel to the phase velocity vector.

The streamlines of the Poynting vector are parallel to one another, i.e., the power flux is laminar. Therefore, the energy velocity can be defined as

$$\overrightarrow{\mathcal{V}}_e = \frac{P}{w}\hat{z}_p, \qquad \mathcal{V}_p = \frac{P}{w}, \tag{40}$$

where

$$P = \sqrt{P_y^2 + P_z^2} = \frac{\sqrt{k_1'^2 + \beta'^2}}{2\omega\varepsilon_0} e^{-2[k_1''(y-a)+\beta'' z]}, \tag{41}$$

is the magnitude of the flux vector and

$$w = \frac{1}{2}[\varepsilon_0|\overrightarrow{E}|^2 + \mu_0|\overrightarrow{H}|^2] = \frac{1}{2}\left[\frac{|k_1|^2 + |\beta|^2}{\omega^2\varepsilon_0} + \mu_0\right] e^{-2[k_1''(y-a)+\beta'' z]}. \tag{42}$$

is the energy volume density. The substitution of eqs. (41) and (42) into eq. (40) gives the following expression for the energy velocity

$$\overrightarrow{\mathcal{V}}_e = \hat{z}_p \frac{\omega\sqrt{k_1'^2 + \beta'^2}}{k_0^2 + |k_1|^2 + |\beta|^2}, \tag{43}$$

or

$$\frac{\overrightarrow{\mathcal{V}}_e}{c} = \hat{z}_p \frac{k_0\sqrt{k_1'^2 + \beta'^2}}{k_0^2 + |k_1|^2 + |\beta|^2}. \tag{44}$$

The absolute values of this ratio are plotted on Fig. 21. At the upper cutoff frequency, $\sqrt{k_1'^2 + \beta'^2} = k_0, |k_1|^2 + |\beta|^2 = k_0^2$, and $\mathcal{V}_e = c/2$ The $z$-component of the energy velocity,

$$(\overrightarrow{\mathcal{V}}_e \cdot \hat{z}) = \frac{\omega\beta'}{k_0^2 + |k_1|^2 + |\beta|^2}, \tag{45}$$

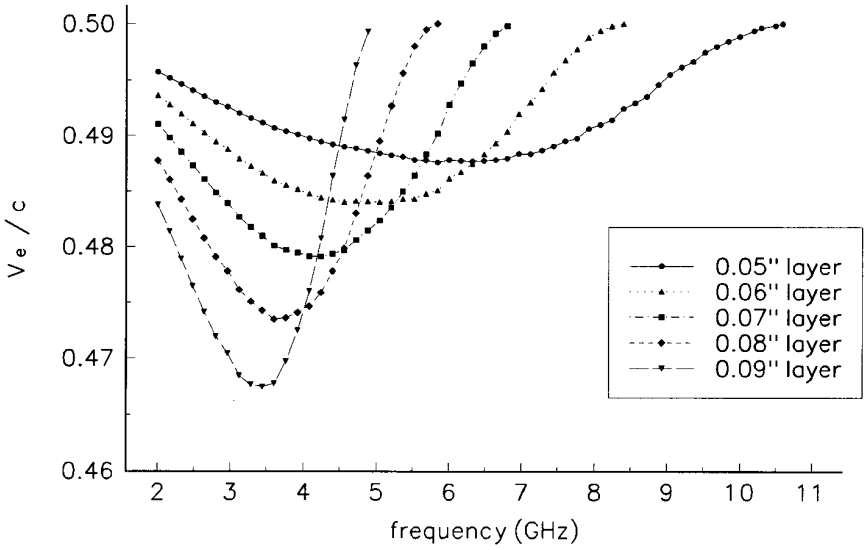


**Figure 21.** Energy velocity outside the layers.

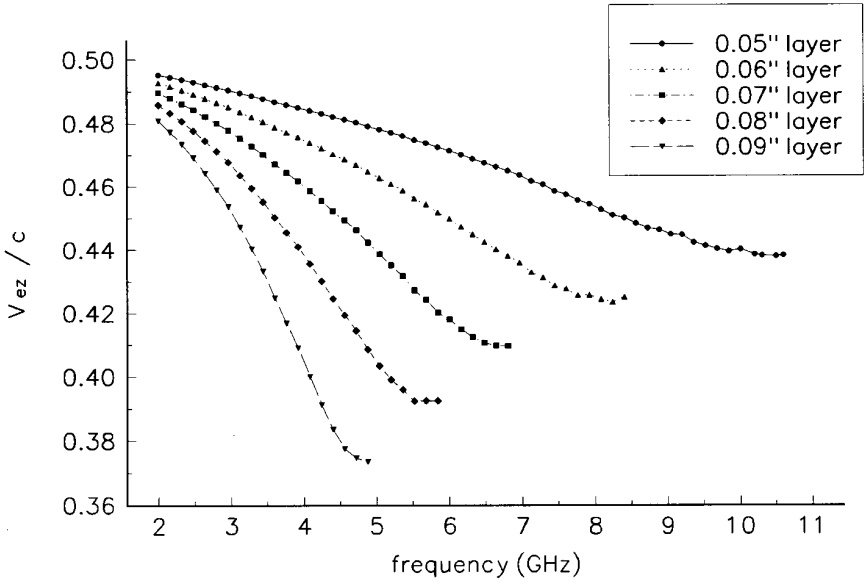


**Figure 22.** The $z$-component of the energy velocity outside the layers.

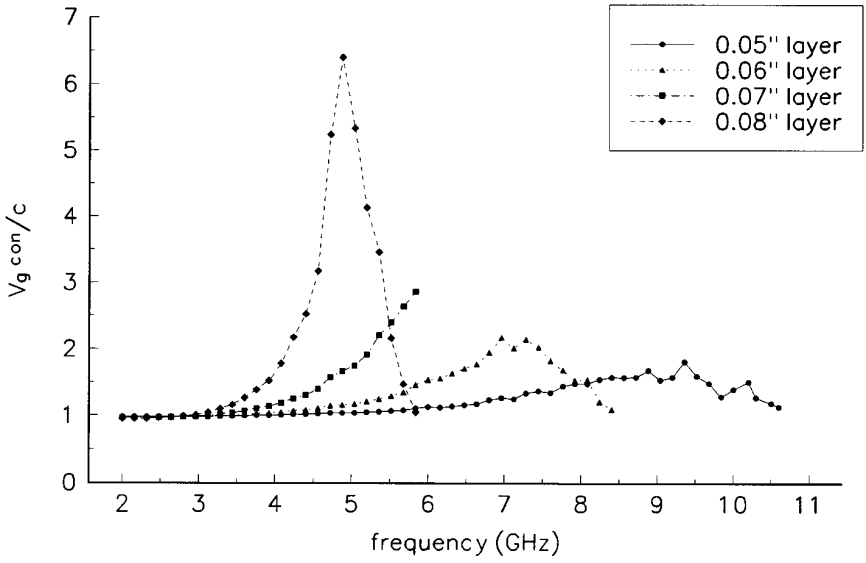


**Figure 23.** Conventional group velocity not applicable to lossy layers.

is plotted on Fig. 22 as a function of frequency. This is completely different from the conventional expression for the group velocity

$$\overrightarrow{\mathcal{V}}_g^{con} = \hat{z}\frac{\partial\omega}{\partial\beta'} = \hat{z}\frac{1}{\partial\beta'/\partial\omega} \tag{46}$$

which leads to absurd values exceeding the light velocity (Fig. 23). Moreover, from Fig. 9, we see that for the thickest layer $(a = 0.09'')$, the curve $\mathrm{Re}(\beta) = \beta'(\omega)$ has the maximum at the frequency about $f = 3.8$ GHz and the minimum near $f = 4.5$ GHz. At the maximum and minimum the derivative $\partial\beta'/\partial\omega$ equals zero and changes its sign. This means that at these frequencies, the conventional group velocity changes its value from $+\infty$ to $-\infty$ at the maximum of $\beta'(\omega)$ and from $+\infty$ to $-\infty$ at the minimum of $\beta'(\omega)$.

The scalar product of the phase and group velocities given by eqs. (34) and (43) becomes

$$\overrightarrow{\mathcal{V}}_p \cdot \overrightarrow{\mathcal{V}}_e = \mathcal{V}_p \cdot \mathcal{V}_e = \frac{\omega^2}{k_0^2 + |k_1|^2 + |\beta|^2} = \frac{c^2}{1 + \frac{|k_1|^2+|\beta|^2}{k_0^2}}. \tag{47}$$

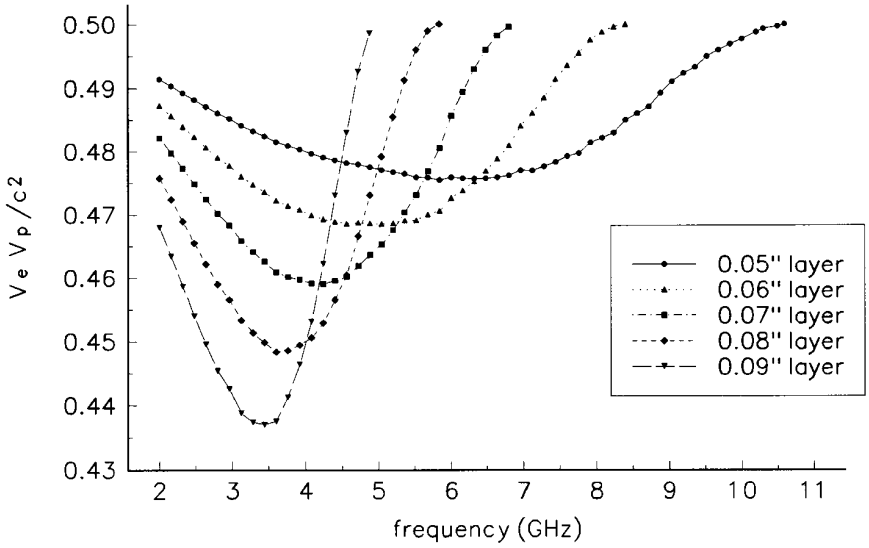


**Figure 24.** Product of energy velocity and phase velocity outside the layers.

The ratio $(\mathcal{V}_p \cdot \mathcal{V}_e)/c^2$ is plotted on Fig. 24. At the upper cutoff frequency this quantity equals 0.5 because $\mathcal{V}_e = c/2$ and $\mathcal{V}_p = c$. It is interesting to note that the scalar product of vector $\overrightarrow{\mathcal{V}}_e$ (Eq. (43)) and $\overrightarrow{\mathcal{V}}_p^{con} = (\omega/\beta')\hat{z}$ is exactly equal to the right-hand side of the eq. (47).

For lossless layers the following relationships hold

$$k_1' = 0, \quad k_1 = ik_1'', \quad \beta'' = 0, \quad \beta = \beta', \quad \gamma_p = \pi/2,$$

$$\sqrt{k_1'^2 + \beta'^2} = \beta, \qquad k_1^2 + \beta^2 = k_0^2 = \beta^2 - (k_1'')^2,$$

$$|k_1|^2 + |\beta|^2 = \beta^2 + (k_1'')^2 = 2\beta^2 - k_0^2,$$

$$k_0^2 + |k_1|^2 + |\beta|^2 = 2\beta^2. \tag{48}$$

As a result, in the case of lossless layers the above eqs. (34) and (43) for the phase and energy velocities reduce to

$$\overrightarrow{\mathcal{V}}_p = \hat{z}\frac{\omega}{\beta}, \qquad \overrightarrow{\mathcal{V}}_e = \hat{z}\frac{\omega}{2\beta} = \frac{1}{2}\overrightarrow{\mathcal{V}}_p. \tag{49}$$

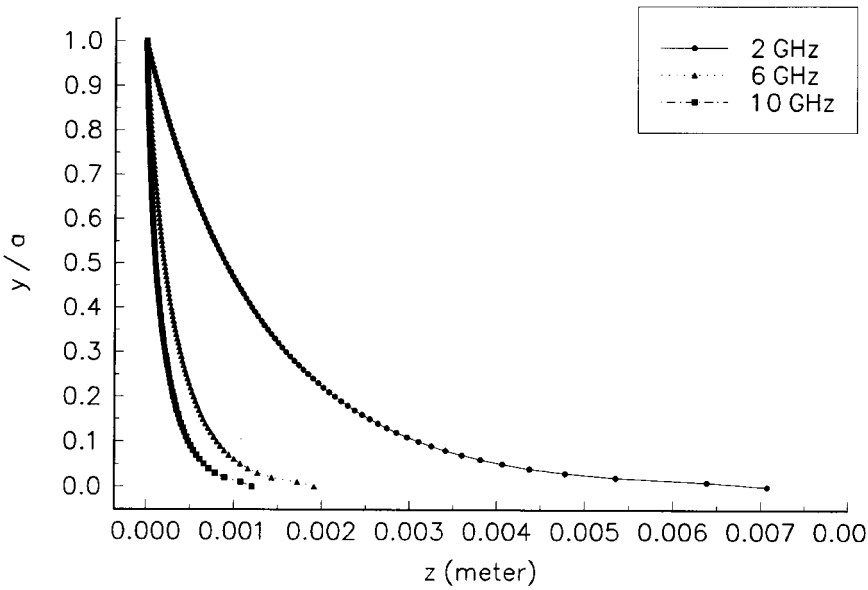


**Figure 25.** Streamlines of the power flux inside the layer. Layer thickness $a = 0.05''$.

Thus in this particular case, the energy velocity is half of the phase velocity.

Unfortunately, it is impossible to apply the above definition (40) for the energy velocity inside the absorbing layers. There is no general expression in electromagnetics for the energy volume density $w$ in absorbing and dispersive media [17, 18]. However, the pattern of the power flux in the absorbing layers can be demonstrated by the streamlines of the Poynting vector. This is shown in Fig. 25. These lines are determined by the equation (Fig. 26)

$$\frac{dz}{dy} = -\tan\varphi(y) \tag{50}$$

where

$$\begin{aligned}\tan\varphi(y) &= -\frac{P_z}{P_y} \\ &= \frac{2(\beta'\varepsilon' + \beta''\varepsilon'')\{[\cos(k_2'y)\cosh(k_2''y)]^2 + [\sin(k_2'y)\sinh(k_2''y)]^2\}}{(k_2'\varepsilon' + k_2''\varepsilon'')\sinh(2k_2''y) + (k_2''\varepsilon' - k_2'\varepsilon'')\sin(2k_2'y)}.\end{aligned} \tag{51}$$

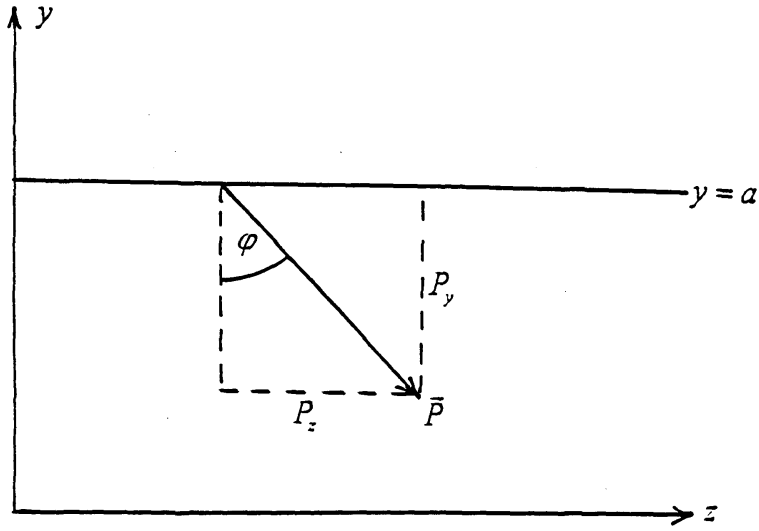


**Figure 26.** Definition of the angle $\varphi(y)$.

The solution of eq. (50) is given by the integral

$$z = \zeta + \int_y^a \tan\varphi(y)dy \tag{52}$$

where $(\zeta, a)$ is an arbitrary point at the layer boundary $y = a$. Because $P_y = 0$ on the perfectly conducting substrate $(y = 0)$, the streamlines are tangential to the $z$ axis. Note that in Fig. 25 only the streamlines passing through the point with initial coordinates $\zeta = 0, y = a$ on the layer surface are shown. The streamlines passing through any other point on the layer surface have exactly the same shape.

## 6. THE SURFACE IMPEDACE OF THIN ABSORBING LAYERS

In this Section we discuss the method of describing the scattering and guiding properties of thin absorbing layers by using the concept of the surface impedance. Suppose that the incident plane wave

$$H_x^{inc} = e^{ik_0(z\cos\theta - y\sin\theta)} \tag{53}$$

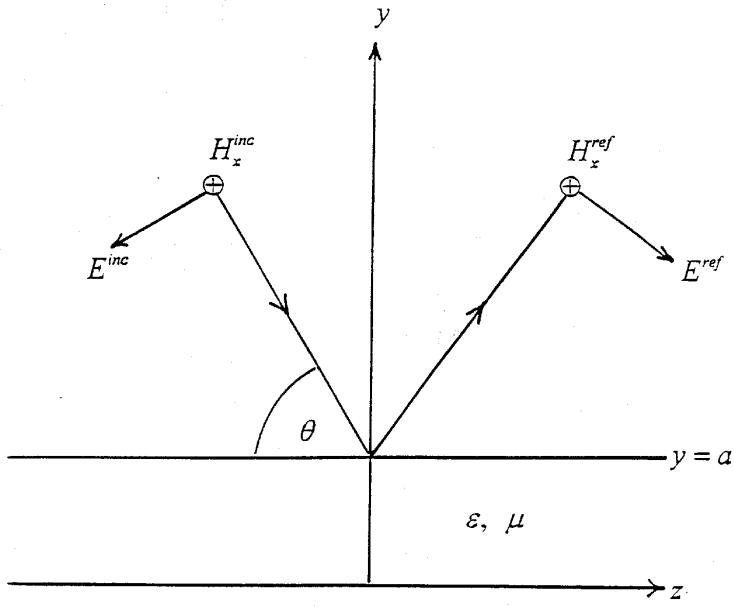


**Figure 27.** Reflection of the plane wave by the layer.

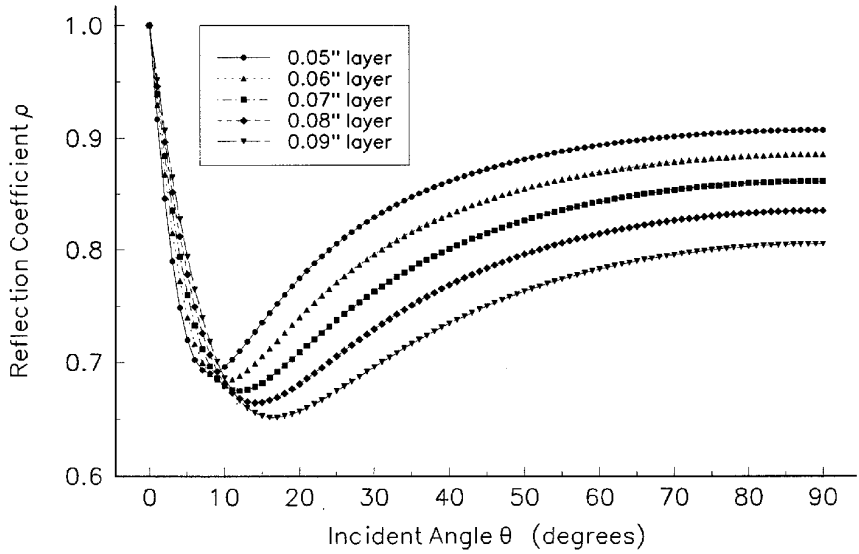


**Figure 28.** Reflection coefficient of plane wave incident on lossy layer. The wave frequency is equal to 2 GHz.

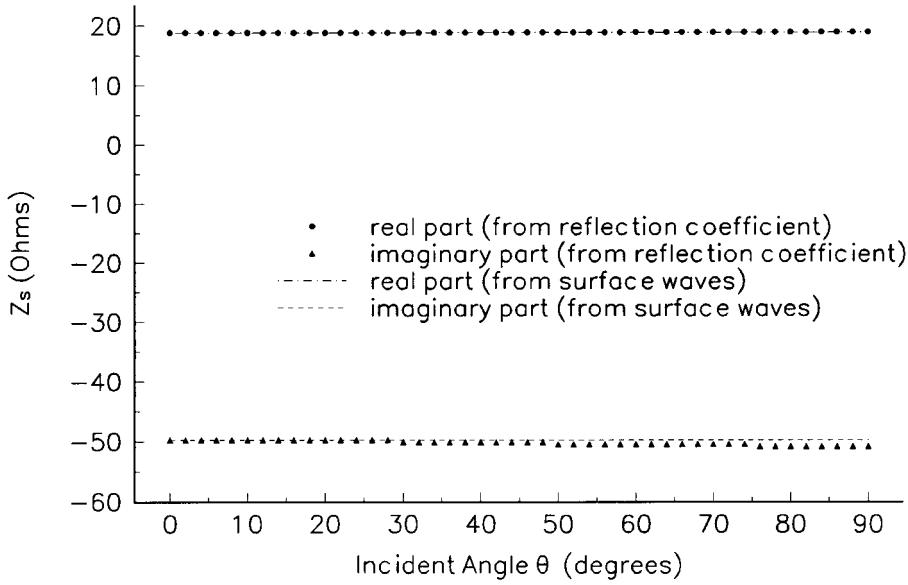


**Figure 29.** Surface impedance. Layer thickness $0.05''$, 2 GHz.

is reflected from the homogeneous absorbing layer (Fig. 27) and transforms into the wave

$$H_x^{ref} = \rho(\theta) e^{ik_0(z\cos\theta + y\sin\theta) - i2k_0 a\sin\theta}. \tag{54}$$

The reflection coefficient $\rho(\theta)$ is given by

$$\rho(\theta) = \frac{\epsilon\sin\theta + i\sqrt{\epsilon\mu - \cos^2\theta}\,\tan(k_0 a\sqrt{\epsilon\mu - \cos^2\theta})}{\epsilon\sin\theta - i\sqrt{\epsilon\mu - \cos^2\theta}\,\tan(k_0 a\sqrt{\epsilon\mu - \cos^2\theta})} \tag{55}$$

where $\epsilon$ and $\mu$ are defined in Section 2. The moduli of this coefficient are shown in Fig. 28. They reach minimum values at certain angles $\theta_{\min}$. Data for the angle $\gamma_p$ (Fig. 11) show that the incidence angles $90^\circ - \theta_{\min}$ are not far from the real part of the complex Brewster angle $(\gamma'_B = \gamma_p)$. For example for the layer with thickness of 0.05 inch, we have $\theta_{\min} \approx 8^\circ$, $90^\circ - \theta_{\min} \approx 82^\circ$ and $\gamma'_B \approx 87^\circ$. What is surprising is that the $\theta_{\min}$ values are close to the imaginary part of the Brewster angle $\gamma''_B$ (Fig. 13).

The ratio

$$Z_s^{ref} = -\frac{E_z^{inc} + E_z^{ref}}{H_z^{inc} + H_z^{ref}} = Z_0 \frac{1-\rho(\theta)}{1+\rho(\theta)} \sin\theta \qquad \text{(Ohm)} \qquad (56)$$

is plotted on Fig. 29. It is nearly constant for all angles of incidence and practically identical to that defined in eq. (7) for surface waves. Thus, we see that those particular layers with large refractive index $n = \sqrt{\epsilon\mu}$ which are considered in the present paper can be described in terms of the surface impedance $Z_s$. This concept is used in the next Section for the solution of the excitation problem.

One should note the connection between the reflection of plane waves from the layers and the surface waves propagating along the same layers. By setting $\cos\theta = \beta/k_0$ and $\sin\theta = -\sqrt{1-(\beta/k_0)^2}$ with complex $\beta$ determined by eq. (6), the incident plane wave given by eq. (53) transforms into eq. (1) for the surface wave. The angle $\theta$ here can be recognized as the complement of the Brewster angle $\gamma_B$ defined by eq. (26). The reflection coefficient changes into

$$\rho_s = \frac{i\epsilon\sqrt{k_0^2-\beta^2} + \sqrt{k_0^2\epsilon\mu-\beta^2}\tan(a\sqrt{k_0^2\epsilon\mu-\beta^2})}{i\epsilon\sqrt{k_0^2-\beta^2} - \sqrt{k_0^2\epsilon\mu-\beta^2}\tan(a\sqrt{k_0^2\epsilon\mu-\beta^2})} \qquad (57)$$

The numerator of this expression is exactly the left-hand side of the dispersion equation (6) and, therefore, it is equal to zero. This confirms the known results [7, 8], that the surface wave can be considered as an inhomogeneous plane wave incident on the guiding structure under the complex Brewster angle without reflection.

## 7. EXCITATION OF SURFACE WAVES ON THE IMPEDANCE PLANE

In the previous Section it is shown that the absorbing layers, studied in this paper, can be considered approximately as infinite planes with the surface impedance $Z_s$ given by eq. (7). The excitation of surface waves on an impedance plane was investigated in details by Cullen, Booker and Clemmow for the Zenneck type surface waves. Their results were summarized by Barlow and Brown in Reference 8. We extend their theory below to the application to lossy layers. The problem is formulated as follows. An external source is located somewhere in the region $-\infty \le x \le \infty$, $0 \le y \le \infty$, $-\infty \le z \le 0$. This source creates

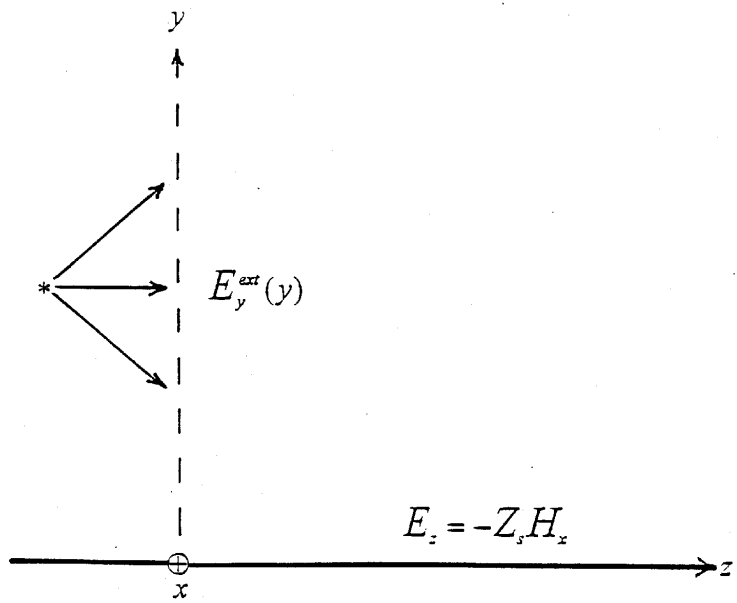


**Figure 30.** Excitation of surface waves over an impedance surface $(y = 0)$.

a field with the $E_y^{ext}$-component in the half-plane $z = 0$, $0 \leq y \leq \infty$, $-\infty \leq x \leq \infty$ above the impedance plane (Fig. 30). Note that in Fig. 30 we placed the coordinate origin on the layer surface to make the equations for the fields simpler. A two-dimensional problem is considered where $E_y^{ext}$ is assumed to be independent of the coordinate $x$ and $Z_s$ is constant for all coordinates $x$ and $z$. The fields excited in the quadrant $0 \leq y \leq \infty$, $0 \leq z \leq \infty$ satisfy the Maxwell equations and the impedance boundary condition, eq. (7). They also satisfy the radiation condition as $r = \sqrt{y^2 + z^2} \to \infty$ with $y \geq 0$, $z > 0$. In addition, the $E_y$-component of the excited field must be equal exactly to the external field $E_y = E_y^{ext}$ in the half-plane $z = 0$, $0 \leq y \leq \infty$.

The solution of the above problem is found by using the concept of plane wave spectrum introduced by Booker and Clemmow [9]. The basic idea is that the solution can be represented as a linear combination of all possible plane waves incident on the interface plane $x$-$z$ including those with complex incident angles. When the solution is specialized to the aperture plane (i.e., $x$-$y$ plane at $z = 0$) where $E_y^{ext}(y)$

is specified, the spectrum of the aperture-limited plane wave acquires components with the complex incident angles necessary for the excitation of surface waves. Both Cullen [13] and Booker and Clemmow [9, 10] provide rigorous solutions to the boundary value problem based on the plane-wave spectrum concept. The former solves the problem by expanding the fields as plane-wave spectra in the region $y \geq 0$ while the latters do the same in the region $z \geq 0$. Barlow and Brown [8] show that these two solutions are mathematically equivalent.

The final complete solution for the $H_x$ component of the magnetic field in the region $0 \leq y \leq \infty$, $0 \leq z \leq \infty$ is given by

$$H_x = -\frac{\omega\epsilon_0}{2\pi}\int_{-\infty}^{\infty}\left[F(\zeta)+\frac{\zeta+k_1}{\zeta-k_1}F(-\zeta)\right]\frac{e^{i(y\zeta+z\sqrt{k_0^2-\zeta^2})}}{\sqrt{k_0^2-\zeta^2}}d\zeta + \frac{2i\omega\epsilon_0 k_1}{\beta}F(-k_1)e^{i(k_1 y+\beta z)}, \tag{58}$$

$$E_y = \frac{i}{\omega\epsilon_0}\frac{\partial H_x}{\partial z}, \qquad E_z = -\frac{i}{\omega\epsilon_0}\frac{\partial H_x}{\partial z}, \tag{59}$$

where

$$F(\zeta) = \int_0^{\infty} E_y^{ext}(y)e^{-i\zeta y}dy \tag{60}$$

is the Fourier transform of the external electric field component in the aperture plane. Note that eq. (58) is opposite in sign to eq. (10.45) in [8] because we use a different system of coordinates.

For the double valued function $\sqrt{k_0^2-\zeta^2}$, the branch with $\mathrm{Im}(\sqrt{k_0^2-\zeta^2}) \geq 0$ is chosen. This insures the convergence of the integral in eq. (58). The branch cuts in the complex plane $\zeta = \zeta' + i\zeta''$ are semi-infinite curves (Fig. 31). The left branch cut extends from the branch point $\zeta = -k_0$ to $\zeta = 0$ and then to $\zeta = -i\infty$. The right branch cut extends from the branch point $\zeta = +k_0$ to the point $\zeta = 0$ and then to $\zeta = +i\infty$. In Fig. 31 these branch cuts are shown in a slightly modified form to better illustrate the location of the integration contour. The directions shown by arrows on the branch cuts allow one to distinguish the left and right side. On the left side, $\sqrt{k_0^2-\zeta^2} > 0$, while on the right side, $\sqrt{k_0^2-\zeta^2} < 0$.

To elicit the physical meaning of each of the terms in eq. (58), we apply it to the case where the prescribed aperture field is generated by a line source located at $y = y_0$. In this case $E_y^{ext} = \delta(y-y_0)$, $F(\zeta) = \exp(-iy_0\zeta)$, and eq. (58) become

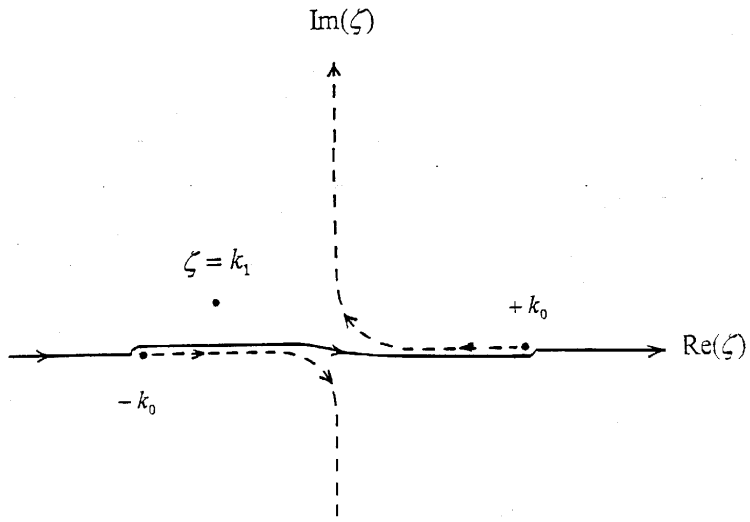


**Figure 31.** Branch cuts in the complex plane $(\zeta)$ and the integration contour in eq. (58).

$$
\begin{aligned}
H_x = &- \frac{\omega\epsilon_0}{2\pi} H_1^{(0)}[k_0\sqrt{z^2+(y-y_0)^2}] \\
&- \frac{\omega\epsilon_0}{2\pi}\int_{-\infty}^{+\infty} \frac{\zeta+k_1}{\zeta-k_1}\exp\{i[\zeta(y+y_0)+z\sqrt{k_0^2-\zeta^2}]\}\frac{d\zeta}{\sqrt{k_0^2-\zeta^2}} \\
&+ \frac{2i\omega\epsilon_0 k_1}{\beta}\exp\{i[k_1(y+y_0)+\beta z]\} \qquad (61)
\end{aligned}
$$

where $H_1^{(0)}(x)$ is the zeroth order Hankel's function of the first kind. The first term on the right hand side of eq. (61) is the direct wave arriving at the observation point from the line source. The second term represents the field reflected by the impedance surface before reaching the observation point. The third term represents the surface wave excited on the impedance surface by the line source. This interpretation becomes obvious when we look at the asymptotic expressions of the first two terms. Let $r^s = \sqrt{z^2+(y-y_0)^2}$ be the distance between the source point and the observation point. As $k_0 r^s \gg 1$, the first term in eq. (61) becomes

$$H_x^{inc} \approx -\omega\epsilon_0 \frac{\exp[i(k_0 r^s - \pi/4)]}{\sqrt{2\pi k_0 r^s}}. \tag{62}$$

Similarly let $r^\star = \sqrt{z^2 + (y + y_0)^2}$ be the distance between the image of the source point as reflected by the impedance surface and the observation point. As $k_0 r^\star \gg 1$, the second term in eq. (61) becomes

$$H_s^{ref} \approx -\omega\epsilon_0 \left(\frac{k_0 \sin\theta + k_1}{k_0 \sin\theta - k_1}\right) \frac{\exp[i(k_0 r^\star - \pi/4)]}{\sqrt{2\pi k_0 r^\star}} \tag{63}$$

where $\theta$ is the angle made by the reflected beam with the $z$-axis. In eq. (63), the quantity $(k_0 \sin\theta + k_1)/(k_0 \sin\theta - k_1)$ can thus be recognized as the reflection coefficient. Its numerical values are nearly identical to those computed from eq. (55) for layers with large refractive indicies.

In view of eqs. (62) and (63), the integrand in eq. (58) can be interpreted as a composition of two spectral components. The one associated with amplitude $F(\zeta)$ corresponds to the incident wave while the other associated with $F(-\zeta)$ corresponds to the reflected wave with the factor $(\zeta + k_1)/(\zeta - k_1)$ being the reflection coefficient of a spectral component of the incident wave. The last term in eq. (58) accounts for the surface wave excited on the impedance surface.

In Section 3 it is shown for the layers considered in this paper that $-k_0 < k_1' < 0$ (Fig. 8) and $k_1'' \to 0$ when the frequency approaches the upper cutoff frequency. In this case, the pole $\zeta = k_1$ reaches the integration contour. With further frequency increase, it intersects the integration contour, moves in the lower half-plane $(\mathrm{Im}(\zeta) < 0)$ through the branch cut, and appears in the next Riemann sheet. The residue, which arises due to the intersection of the integration contour cancels the last term in eq. (58) and the surface wave disappears. This is also quite natural from the physical point of view. At the upper cutoff frequency the surface wave transforms into the plane wave transmitting an infinite energy. Finite power source cannot generate such a wave. This is another confirmation of the upper cutoff phenomenon in absorbing layers. In the case of this phenomenon, the total excited field is described by the integral

$$H_x = -\frac{\omega\epsilon_0}{2\pi} \int_{-\infty}^{+\infty} \left[F(\zeta) + \frac{\zeta + k_1}{\zeta - k_1} F(-\zeta)\right] \frac{e^{i(y\zeta + z\sqrt{k_0^2 - \zeta^2})}}{\sqrt{k_0^2 - \zeta^2}} d\zeta \tag{64}$$

and consists of the radiation from the aperture and its reflection from the layer. One should note that at above the cutoff frequency even the cutoff surface wave $E_y^{ext} = \exp(ik_1 y)$ impressed in the limited aperture $(z = 0,\ 0 \le y \le a < \infty)$ cannot excite the surface wave and can create only the radiated and reflected fields. A special case of the field excitation above a homogeneous conducting ground plane by an aperture limited surface wave (below the upper cutoff frequency) is considered in details by Hill and Wait [19].

## 8. LAUNCHING EFFICIENCY OF SURFACE WAVES EXCITED BY APERTURE-LIMITED PLANE WAVES

In this Section we apply the above theory to the case when the absorbing layer is excited by the plane wave

$$\begin{aligned} H_x^{ext} &= e^{-ik_0 y \sin\theta}, \\ E_y^{ext} &= -Z_0 \cos\theta e^{-ik_0 y \sin\theta}, \\ E_z^{ext} &= -Z_0 \sin\theta e^{-ik_0 y \sin\theta} \end{aligned} \tag{65}$$

limited by the aperture $0 \le y \le h$, $z = 0$ on the $x$-$y$ plane (Fig. 32). Outside the aperture in the half-plane $z = 0$, $h \le y \le \infty$ the external field is zero, i.e., $E_y^{ext} = 0$. From the physical point of view this means that the surface $z = +0$, $h \le y \le \infty$ is assumed to be perfectly conducting. The function $F(\zeta)$ in eq. (58) becomes

$$F(\zeta) = iZ_0 \frac{\cos\theta}{k\sin\theta + \zeta}[1 - e^{-i(k\sin\theta+\zeta)h}]. \tag{66}$$

The launching efficiency can be defined as the ratio

$$\eta = \frac{P_1 + P_2}{P^{inc}} \tag{67}$$

where $P_1$ and $P_2$ are the total power fluxes transmitted by the surface wave, respectively, outside and inside the layer across the surface $z = 0$. The quantity $P^{inc}$ is the power flux transmitted by the incident plane wave across the aperture. These quantities are determined by the following expressions

$$P^{inc} = \frac{1}{2} Z_0 h \cos\theta\ , \tag{68}$$

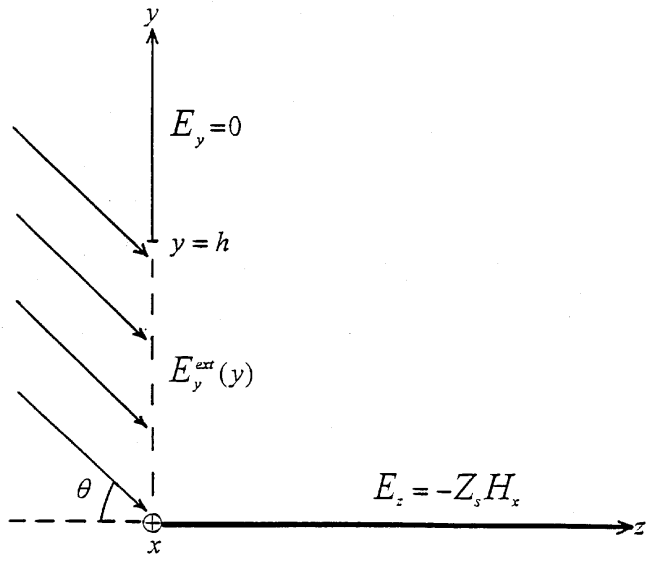


**Figure 32.** Excitation of surface waves by an aperture-limited plane wave.

$$P_1 = \omega\epsilon_0 \frac{\beta'}{k_1''} \left|\frac{k_1}{\beta}\right|^2 \cdot |F(-k_1)|^2, \tag{69}$$

$$P_2 = 2\omega\epsilon_0 \mathrm{Re}\left(\frac{\beta}{\epsilon}\right) \left|\frac{k_1}{\beta}\right|^2 \cdot |F(-k_1)|^2 \frac{\int_0^a |\cos(k_2 y)|^2 dy}{|\cos(k_2 a)|^2}. \tag{70}$$

The integral in (70) is expressed through elementary functions by eq. (20).

Numerical values for launching efficiency $\eta$ are shown in Fig. 33. They are at maximums for the grazing incidence ($\theta = 0°$) and monotonically decrease, approaching zero for the normal incidence ($\theta = 90°$). When the incidence angle $\theta$ exceeds $10°$ the launching efficiency of the surface wave becomes less than 10% as it is the case for all layers. The ratio $P_2/P_1$, which is independent of launching height and plotted on Fig. 34, shows that more than 99.5% of the total power transmitted by the surface wave is concentrated outside the layer. Figure 35 allows one to compare these powers with the power $P^{ref} = |\rho(\theta)|^2 P^{inc}$ which is reflected from the layer. The latter always dominates. The total power transmitted by the surface wave does not exceed 43% of the reflected power for the thinnest layer ($a = 0.05''$)

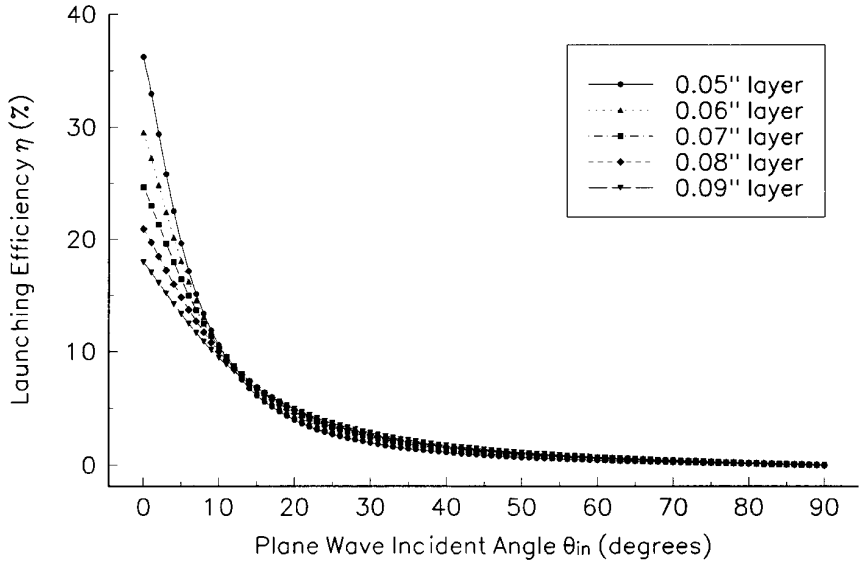


**Figure 33.** Launching efficiency at 2 GHz. Launching height 1 meter.

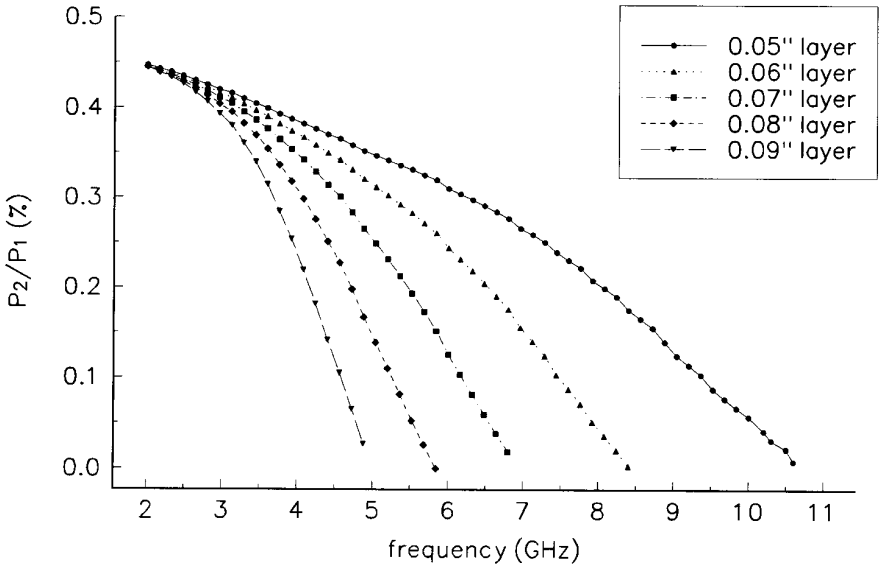


**Figure 34.** $P_2/P_1$ ratio.

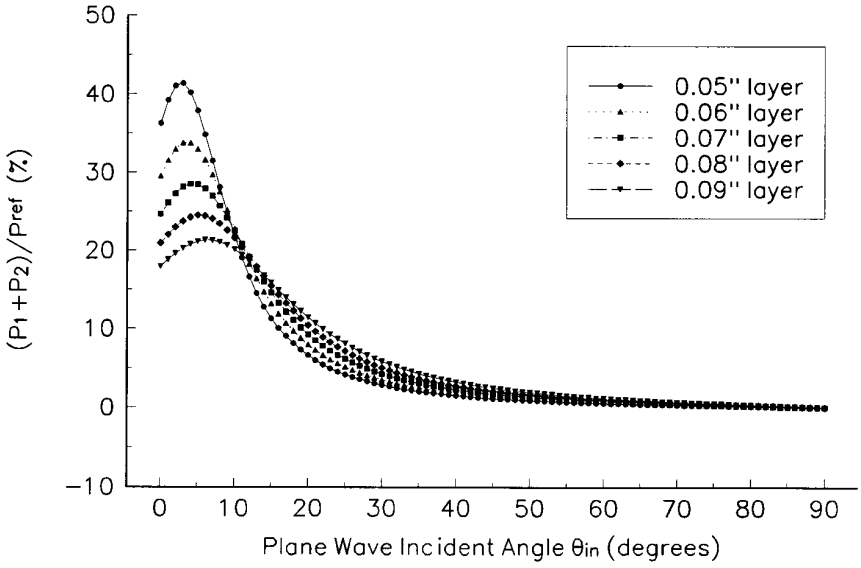


**Figure 35.** $(P_1+P_2)/P^{ref}$ ratio at 2 GHz. Launching height 1 meter.

and 23% for the thickest layer $(a = 0.09'')$. This occurs in the interval $5^\circ < \theta < 10^\circ$. For angles $\theta > 10^\circ$, the ratio $(P_1 + P_2)/P^{ref}$ does not exceed 20% and monotonically approaches zero at $\theta = 90^\circ$.

## 9. SUMMARY AND CONCLUSION

Surface waves propagating along thin absorbing layers with a perfectly conducting substrate have been investigated in this paper. Complex permittivity and permeability of layers measured in the frequency band 2 to 18 GHz and shown in Fig. 2 are used as the basis of computations. Thickness of layers ranges from 0.05 to 0.09 inches. The layers and substrate are infinite in length and width.

A main result is the discovery of an upper cutoff frequency for surface waves (Sec. 3, Figs. 3-5). This phenomenon does not exist in the case of isotropic lossless layers. It was known probably only for magneto-static surface waves on lossless ferrite substrates [14]. However, a difference in principle exists between surface waves on an absorbing isotropic layer and magneto-static surface waves. The phase velocity of surface waves tends to light speed (Fig. 17) while the phase

velocity of magneto-static waves tends to zero when the wave frequency approaches the upper cutoff frequency (Fig. 2 in [14]). The frequency band of surface waves depends on the layer thickness. The thinner the layer the wider this frequency band becomes (Figs. 3–5, 7). In this frequency band the surface waves are fundamental modes. This follows from the inequality $k_2' a < \pi/2$ which was verified numerically.

Figure 7 deserves special attention. It is to be noted that the $k_2' a$ values shown there are for the frequency at 18 GHz. The figure exhibits that the negative (non-physical) wave numbers reach minimum values and then increase with the tendency to become positive again. This suggests that the second mode surface wave can propagate along the layer at higher frequencies. Since the fundamental mode is cutoff at these frequencies, the second mode will be a single mode. This is in contrast with the case of lossless layers which allow the simultaneous propagation of the second and fundamental modes.

One more interesting observation follows from Fig. 7 if we take into account the connection between TM- and TE-surface waves. The surface impedance of TM-waves is determined by eq. (7). We represent it now as $Z_s^{TM} = -(k_1^{TM}/k_0)Z_0$. The surface impedance for TE-surface waves equals $Z_s^{TE} = -(k_0/k_1^{TE})Z_0$. For a truly isotropic impedance surface, the equality $Z_s^{TE} = Z_s^{TM}$ is valid which leads to the relationship $k_1^{TE} k_1^{TM} = k_0^2$. Thus, the wave numbers $k_1^{TE}$ and $k_1^{TM}$ always have imaginary parts with opposite signs. TM-waves can propagate over the inductive surface $[\mathrm{Im}(k_1^{TM}) > 0]$ while TE-waves can propagate over the capacitive surface $[\mathrm{Im}(k_1^{TE}) < 0]$. Therefore the frequency band forbidden for TM-surface waves is allowed for TE-waves and vice versa. This means that the frequency band with negative values $k_1''$ shown in Fig. 7 is allowed for TE-surface waves. In addition the relationship $k_1^{TE} = k_0^2/k_1^{TM}$ together with eq. (3) rewritten for TE-case allows one to find all wave numbers for TE-waves if the quantity $k_1^{TM}$ is known. In other words all characteristics of TE-waves can be found readily if those for TM-waves are known and vice versa. For realistic layers, $Z_s^{TE}$ is equal to $Z_s^{TM}$ only approximately, so are $k_1^{TE}$ and $k_0^2/k_1^{TM}$.

More than 99% of the power transmitted by surface waves along absorbing layers is concentrated outside the layer (Fig. 34). The energy absorption inside the layers reveals a resonance behavior, approaching maximum values for the layer thickness about $0.19\lambda_d$ - $0.20\lambda_d$ (Fig. 6) where $\lambda_d = \lambda_0/\mathrm{Re}(\sqrt{\varepsilon\mu})$ and $\lambda_0$ is the wavelength in free space.

The energy velocity *outside the layers* is defined as the ratio $\overrightarrow{\mathcal{V}}_e = \overrightarrow{P}/w$ where $\overrightarrow{P}$ is the time-averaged Poynting vector and $w$ is the time-averaged energy volume density. The explicit expressions for $\overrightarrow{\mathcal{V}}_e$, are given by eqs. (43) and (44) in Section 5. This vector is perpendicular to the phase front and is directed into the layer. It makes an angle $\gamma_a = (\pi/2) + \gamma_p$ with the layer surface (Figs. 10, 12) where $\gamma_p = \gamma'_B$ (Fig. 11) is the real part of the complex Brewster angle defined by eqs. (27) and (28).

The quantity $\overrightarrow{\mathcal{V}}_e$ is always less than the light speed (Fig. 21) while the conventional group velocity $\mathcal{V}_g^{con} = \partial\omega/\partial\beta'$ is greater than the light speed (Fig. 23). The quantity $\overrightarrow{\mathcal{V}}_g^{\,con}$ can even acquire infinite values and change sign when the real part of the propagation constant $\beta'(\omega)$ as a function of frequency contains a maximum, minimum, or inflection point (Fig. 9). The definition of conventional group velocity is thus non-physical and cannot be applied to lossy and dispersive layers. The product of the phase and energy velocities is determined by the simple eq. (47) and illustrated in Fig. 24.

The excitation of surface waves in absorbing layers is considered in the impedance surface approximation (Sec. 7). This approach is justified by numerical calculations of the ratio $E_z/H_x$ where $E_z$ and $H_x$ are tangential components of the total field induced by the incident plane wave on the layer surface. It is found that this ratio is practically independent of the incidence angle (Fig. 29). Maximum launching efficiency of surface waves by the aperture-limited plane wave occurs near grazing incidence (Fig. 33). It is highest for the thinnest layer and does not exceed 37%.

The results of this paper can be used in the study of scattering from objects with planar facets coated by thin absorbing layers. Among such objects, an interesting example is a cavity with flat coated walls. The theory developed in the paper can be generalized to anisotropic absorbing layers. As it is shown in [15], the inhomogeneous plane waves in anisotropic conducting media reveal some interesting properties. In particular they cannot propagate in certain directions. Because inhomogoneous plane waves are constituent components of surface waves, one can also expect a special behavior of surface waves in anisotropic absorbing layer with a frequency dispersion.

## REFERENCES


1. Sommerfeid, A., "Fortpflanzung electrodynamischer Wellen an einem zylindrischen Leiter (Transmission of electrodynamic waves along a cylindrical conductor)," *Annalen der Physik und Chemie,* Vol. 67, 233–290, 1899.
2. Sommerfeld, A., "Über die Ausbreitung der Wellen in der dratlosen Telegraphie (On the propagation of waves in the wireless telelegraphy)," *Annalen der Physik,* Series 4, Vol. 28, 665–736, 1909.
3. Zenneck, J., "Über die Fortpflanzung ebener elektromagnetischer Wellen längs einer ebenen Leiterfläche und ihre Beziehung zur dratlosen Telegraphie (On the propagation of plane electromagnetic waves along a planar conductor surface and its relationship to wireless telegraphy)," *Annalen der Physik,* Series 4, Vol. 23, 848–866, 1907.
4. Goubau, G., "Surface waves and their application to transmission lines," *J. Applied Physics,* Vol. 21, 1119–1128, 1950.
5. Goubau, G., "Single-conductor surface wave transmission lines," Proc. I.R.E., Vol. 39, 619–624, 1951.
6. Goubau, G., "On the excitation of surface waves," *ibid.,* Vol. 40. 865–868, 1952.
7. Stratton, J. A., *Electromagnetic Theory,* McGraw Hill, New York, 1941.
8. Barlow, H. M., and J. Brown, *Radio Surface Waves,* Oxford University Press, London, 1962.
9. Booker, H. G., and P. C. Clemmow, "The concept of an angular spectrum of plane waves and its relation to that of polar diagram and aperture distribution," *Proc. I.E.E.,* Vol. 97, 11–17, 1950.
10. Booker, H. G., and P. C. Clemmow, "A relation between the Sommerfeid theory of radio propagation over a flat Earth and the theory of diffraction at a straight edge," *ibid.,* 18–27.
11. Clemmow, P. C., *Plane Wave Spectrum Presentation of Electromagnetic Field,* Pergamon Press, Now York, 1966.
12. Attwood, S. S., "Surface wave propagation over a coated plane conductor," *J. Applied Physics,* Vol. 22, 504–509, 1951.
13. Cullen, A. L., "The excitation of plane surface waves," *Proc. I.R.E.,* Vol. 101, 225–234, 1954.
14. Yang, H. Y., J. A. Castanoda, and N. G. Alexopoulos, "Surface wave modes of printed circuits on ferrite substrates," *IEEE Trans. MTT,* Vol. 40, No. 4, 613–621, 1992.
15. Carcione, J. M., and F. Cavallini, "Forbidden directions for TM-waves in anisotropic conducting media," *IEEE Trans. AP*, Vol. 45, No. 1, 133–139, 1997.

16. Wait, J. R., *Electromagnetic Waves in Stratified Media,* IEEE Press, New York, 1996.
17. Vainshtein, L. A., Chapter 1 in *Electromagnetic Waves,* Published by Radio i Svyaz, Moscow, 1988 (in Russian).
18. Collin, R. E., Section 2.5 in *Foundation for Microwave Engineering*, McGraw Hill, New York, 1966.
19. Hill, D. A., and J. R. Wait, "Excitation of the Zenneck surface wave by a vertical aperture," *Radio Science,* Vol. 13, No. 6, 969–977, 1978.